The Stochastic Nature of Deformation Twinning: Application to HCP Materials

Irene J. Beyerlein and M. Arul Kumar

Contents

I. J. Beyerlein (✉)
Mechanical Engineering Department, Materials Department, University of California, Santa Barbara, CA, USA
e-mail: beyerlein@ucsb.edu; beyerlein@engineering.ucsb.edu

M. Arul Kumar
Materials Science and Technology Division, Los Alamos National Laboratory, Los Alamos, NM, USA
e-mail: marulkr@lanl.gov; marulkr@gmail.com

W. Andreoni, S. Yip (eds.), *Handbook of Materials Modeling*,
https://doi.org/10.1007/978-3-319-42913-7_103-1

Abstract

Deformation twinning is an important mode of plastic deformation in hexagonal close-packed (HCP) materials. Experimental observations indicate that these twins occur heterogeneously across the polycrystalline microstructure during deformation. The variation is too substantial to be authentically represented by average values, advocating the use of statistical analyses and stochastic models in the studies of HCP material deformation response. This chapter reviews recent efforts to explain the origin of the stochastic nature of twinning and to analyze and simulate deformation twinning in HCP materials from this perspective.

1 Introduction

Hexagonal close-packed (HCP) polycrystals deform by two mechanisms: the glide of dislocations and expansion of deformation twins (Beyerlein et al. 2014; Partridge 1967; Yoo 1981; Yoo and Lee 1991). Both dislocations and twins are confined to proceed on particular crystallographic planes and directions in a given crystal. To deform the crystal, dislocations glide on these planes. Twins, on the other hand, shear the atoms on these planes causing them to reposition into a configuration that is crystallographically reoriented from the original crystal. The high-resolution transmission electron microscopy (HR-TEM) image in Fig. 1a shows the twin-parent relationship for $\{10\bar{1}2\}$ tensile twin in HCP Zr and is illustrated in Fig. 1b. Strain is imposed as the twin domain grows in size (Beyerlein and Tome 2010; Capolungo et al. 2009; Kumar et al. 2018). Compared to slip, twins greatly affect the mechanical response (Proust et al. 2007; Salem et al. 2006; Wang et al. 2013a; Wronski et al. 2018), formability and ductility (Barnett 2007a, b; Kumar et al. 2017d), and failure mechanisms (Simkin et al. 2007; Yang et al. 2008; Yin et al. 2008) of HCP metals. Figure 1c presents a typical example of how twinning can affect the mechanical response of an HCP alloy (AZ31 Mg) (Wang et al. 2013a). As shown, many details, such as yield stress, strain hardening, and ultimate strength, are affected by twinning.

Both mechanisms, slip and twinning, occur heterogeneously across the crystal. Heterogeneity in slip is evident at nanometer to micron scales. Dislocations glide in arrays within slip bands that are nanometers in thickness. As deformation proceeds, dislocations can form patterns consisting of dislocation-rich areas separating nearly dislocation-free areas (Agnew et al. 2002; Akhtar and Teghtsoo 1971; Bay et al. 1992; Hughes and Hansen 1997; Kuhlman-wilsdorf and Hansen 1991; Kuhlmann-Wilsdorf 1999; Kumar and Mahesh 2012). Highly resolved microscopy techniques,

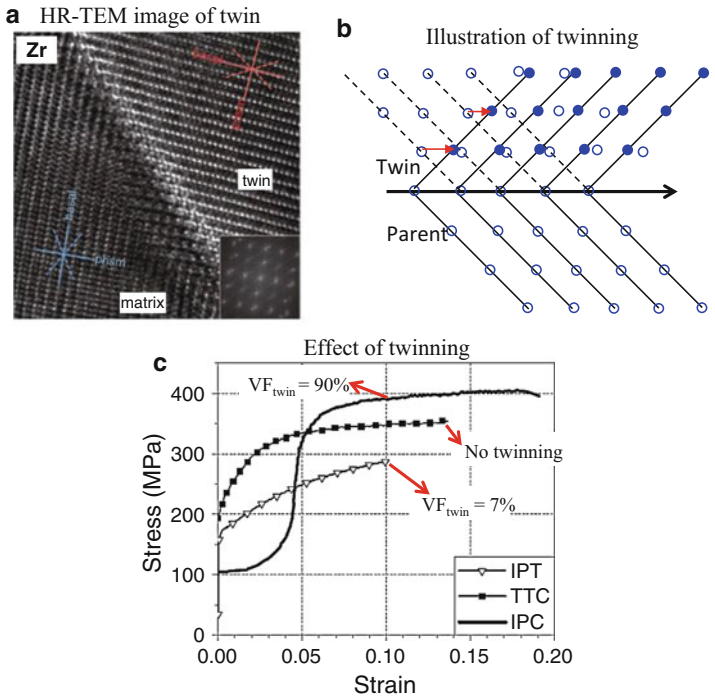

Fig. 1 (**a**) High-resolution TEM image of the twin-parent orientation relationship for the {1012} twin in HCP Zr (Morrow et al. 2014c). (**b**) Schematic of the shearing of atoms that form the twinned lattice from the parent lattice. (**c**) Example showing the effect of deformation twinning on the stress-strain response of HCP AZ31 Mg alloy (Wang et al. 2013a)

such as TEM, can be used to observe individual dislocations and patterns of dislocations within deformed grains and grain boundaries.

Compared to slip, however, the heterogeneity in twinning is evident at much larger scales, such as those of the polycrystal (Barnett et al. 2012; Beyerlein et al. 2010; Capolungo et al. 2009; Kumar et al. 2018; Wang et al. 2013c). The nonuniform nature of twinning can be easily recognized at the resolution of most standard microscopy and diffraction techniques, such as EBSD and optical microscopy. For instance, for Mg (c/a = 1.624), the twin reorientation and local shear associated with the most common tensile twin is 86° and ∼13%, respectively. Large sections of one grain can contain multiple twin domains, whereas another grain of seemingly similar properties (size, shape, orientation) contains no twins. Even in the same grain, the twin thickness can vary easily by two or three times. Twins can expand into neighboring grains. At this larger polycrystal scale, the heterogeneity in dislocation slip would not be discernable.

The widespread heterogeneity in twinning has motivated the use of statistical analyses to understand the role of microstructure, such as grain orientation and grain size, on twinning (Barnett et al. 2012; Beyerlein et al. 2010; Capolungo

et al. 2009; Kumar et al. 2018; Wang et al. 2013c). The apparent sensitivity to local heterogeneities in stress has inspired the use of in-situ testing and simulation techniques to reveal how twin lamella form and expand within a polycrystalline microstructure during deformation (Cheng and Ghosh 2015, 2017a, b; Hazeli et al. 2013; Khosravani et al. 2015; Morrow et al. 2014a, b, c; Wang et al. 2010a, 2011, 2012, 2013b; Wu et al. 2016). Many crystal plasticity models have advanced to incorporate the stochasticity in twin formation and growth, finding better agreement in stress-strain response and microscopy data than the conventional deterministic approach for twin activation (Abdolvand et al. 2015a, b; Abdolvand and Wilkinson 2016; Ardeljan et al. 2015; Beyerlein et al. 2011, 2012; Beyerlein and Tome 2010; Kumar et al. 2017b; Niezgoda et al. 2013, 2014).

The aim of this chapter is to summarize the recent advancements in understanding the formation and growth of deformation twins and likely explanations for the apparent stochastic nature of deformation twinning. The chapter is structured as follows. It begins with a brief review of statistical analyses of large microstructural data sets of materials that twinned during deformation. Next, the modeling methods that have been used to date to simulate twins in HCP polycrystals are briefly introduced. The chapter ends with examples from these calculations and key findings on the role of microstructure and local stresses on twin formation, propagation, and growth.

2 Twinning as a Stochastic – Sequential Process

Statistical analysis of twin and stochastic analysis of twinning dynamics can be used as a way toward better understanding of twinning. For many decades, analyses of microscopy data and deformation models have taken a deterministic approach to treating deformation twinning and only recently have they incorporated stochastic aspects, showing noticeable improvements in prediction. The statistical analyses and companion modeling efforts will be discussed in the following sections.

2.1 Dynamic Processes of Twinning

The twinning process can be viewed broadly as taking place in three stages. Witnessing these stages in situ is challenging, and in lieu of displaying actual experimental images, a schematic of these stages is provided in Fig. 2, where for simplicity only one twin in one grain is shown. Stage 1 is the creation of an embryo (nucleation), which begins at the atomic scale. Twin nucleation models assume that the twinning partials, needed to create a twin embryo, form directly from the dissociation of pre-existing dislocations. The initiating dislocations may be lattice dislocations (Capolungo and Beyerlein 2008; Cohen and Weertman 1963; Jagannadham 1976; Mahajan and Chin 1973; Mendelson 1972; Priestner and Leslie 1965) or dislocations found in grain boundaries (Barrett and El Kadiri 2014; Beyerlein et al. 2011, 2012; Wang et al. 2014) or moving dislocations that have impinged on bi-phase interfaces (Beyerlein et al. 2013; Zheng et al. 2012). The

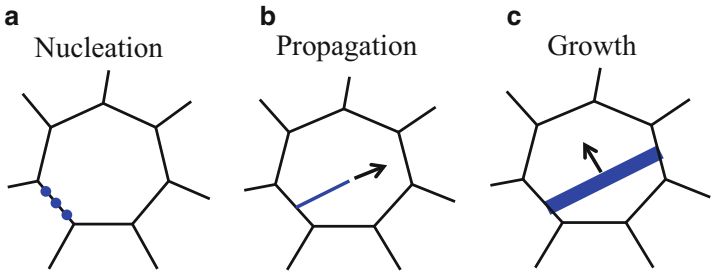

Fig. 2 Schematic showing three basic sequential steps involved in the formation of twin lamella (Kumar et al. 2015). (**a**) Nucleation, formation of twin nuclei at a given grain boundary; (**b**) propagation, propagation of a twin nucleus into the parent crystal; (**c**) growth, migration of the twin boundary and thickening of the lamella

stresses needed to support these reactions are relatively high, requiring localized stress concentrations, generated for example, at the head of dislocation pile ups.

Stages 2 and 3 involve twin growth and the migration of twin boundaries. In stage 2, growing twin embryos, initially nanoscale to submicron in size, propagate under stress into the grains, often spanning the entire crystal and terminating at the other grain boundaries bounding the same grain (Beyerlein and Tome 2010; Capolungo et al. 2009; Kumar et al. 2018; McCabe et al. 2009). In stage 3, these terminated twins begin to propagate and expand. They can grow either by thickening, so their width increases or by transmitting, a process by which a second twin forms on the other side of the grain boundary where the first twin and grain boundary meet.

Both twin nucleation and expansion can occur only if the combination of required stresses and sufficient density of defects are present. Both aspects, mechanical and material in nature, can vary statistically in space and in time in a deforming microstructure and can result in the statistical appearance of a twin or twins in a grain.

2.2 Statistical Features of Deformation Twins

In a polycrystal, grains vary in size, crystallographic orientation, and local grain neighborhood. Most commonly considered microstructural variables that affect the propensity for twinning are grain orientation, grain size, and grain neighborhoods. Using EBSD, twins of thicknesses greater than ~10 nm can be easily seen. As mentioned earlier, analyses of twins using EBSD data on deformed materials typically find twin lamellae that span the grain completely and are bound by grain boundaries.

Due to the statistical nature of twinning, in order to develop reliable statistical correlations between twin properties and grain microstructure from EBSD data, thousands of grains and twins would need to be analyzed. With the advent of automated EBSD techniques, a twinning microstructure that has formed in thousands of

deformed grains can be assessed relative rapidly facilitating creation of statistically significant data sets. With such data, statistical analyses have been carried out to identify correlations between properties of the twinning microstructure (variant, twin thickness) with the grain microstructure (grain size, grain orientation, and grain neighborhood).

In recent years, statistical analyses of twins have been carried out on a number of HCP metals, Mg, Zr, and Ti, and also Mg alloys (Barnett et al. 2012; Beyerlein et al. 2010; Capolungo et al. 2009; Ghaderi and Barnett 2011; Juan et al. 2015; Kacher and Minor 2014; Khosravani et al. 2015; Kumar et al. 2016a, 2017c, 2018; Shi et al. 2015a, c; Tsai and Chang 2013). The general finding is that while grain size and grain orientation can be strongly correlated with the propensity of twinning, the correlations are not as strong as those expected from a deterministic point of view. For instance, the following are found: (1) not all favorably oriented grains twin, (2) some not favorably oriented grains twin, (3) only 40% of twin variants have highest Schmid factor, (4) not all grains of the same orientation twin, (5) twinned grains contain variable numbers of twins, (6) not all grains of the same size twin, and (7) twins have variable thickness.

To elucidate the statistical variation in twinning grain to grain, the statistical results of $\{10\bar{1}2\}$ tensile twin in HCP Mg and Zr are discussed in the following sections. The materials examined are high-purity polycrystalline Mg and Zr with similar initial textures and, hence, similar grain misorientation distributions (Beyerlein et al. 2010; Capolungo et al. 2009). The Mg has a strong basal texture resulting from rolling, where most of the basal poles are aligned within 30° of the normal direction of the sheet. The Zr has a similar strong basal texture, which was developed via clock rolling rather than conventional rolling (Kaschner et al. 2006). Both materials were compressed at 10^{-3}/s in an in-plane direction to activate $\{10\bar{1}2\}$ twinning. In order to develop a sufficient number of incipient twins in many grains, Zr was compressed at 77 K to 10% strains, and Mg was compressed at room temperature to 3% strain. Figure 3 shows the sample EBSD images of the twinning microstructure of the deformed Mg and Zr. Using an automated EBSD software, large data sets were generated by analyzing several distinct EBSD scans (Beyerlein et al. 2010; Capolungo et al. 2009). The number of grains and twins investigated totaled 2339 and 8550 for Mg, and 639 and 1065 for Zr.

2.3 Statistical Analysis of Crystallographic Orientation Effects

Grains are considered to be well oriented for twinning by a given twin type if they have one or more of the six twin variants bearing a high Schmid factor (e.g., >0.33). From a deterministic viewpoint, the twin variant in a grain most likely to form is the one that has the highest Schmid factor. The Schmid factor (SF) of observable twins is the most common parameter quoted in association with twinning. This reference is especially true when discussing whether twin activation obeys an "Schmid criterion," that is, one that is activated by a resolved shear stress in the twin plane and in the twinning direction (TRSS). The SF is defined as the ratio

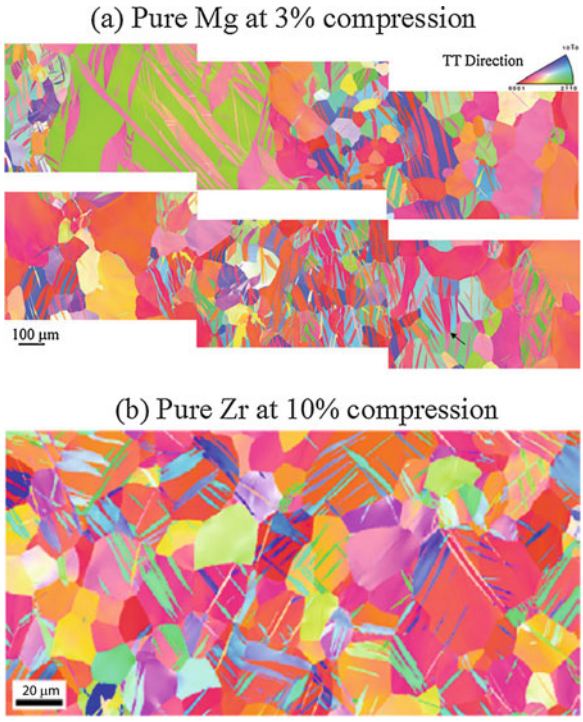

Fig. 3 Sample EBSD images of deformed (**a**) Mg and (**b**) Zr metals showing the activation of tensile twining (Beyerlein et al. 2010; Capolungo et al. 2009). To activate sufficient number of twins, Mg and Zr samples compressed along rolling direction to 3% at RT and to 10% at 77 K, respectively

between the TRSS and the value of the macroscopic tensile or compressive stress. The SF varies between −0.5 and 0.5. It provides a geometric measure of how well a twin system is oriented with respect to an external axial stress. Twins belonging to a given grain are classified by their variant and its rank, 1–6, in decreasing order of their SF. If twin activation obeys a Schmid criterion based on the macroscopic applied stress, the twin would correspond to variant 1, the variant having the highest SF among the six in a grain. In this section, the effect of grain orientation as reflected by its SF on twinning formation, growth, and variant selection is discussed.

Figure 4a plots the twinning frequency taken from large data sets on twinned Mg and Zr. The analysis indicates that for both Zr and Mg, the frequency of twinning increases with SF, which is to be expected. However low SF twins are also activated. Figure 4c, d shows the distribution of twin variants as a function of twin SF for Mg and Zr, respectively. The frequency of each twin variant (1–6) is 35.6%, 23.5%, 21.3%, 11.7%, 3.2%, and 4.6%, respectively, in Mg. Similar frequency in Zr is 49.8%, 20.0%, 17.9%, 8.2%, 3.3%, and 0.7%. It is surprisingly common, among EBSD studies on twinned microstructures, to find that the twin variant selected is not the one with the highest Schmid factor or even the second highest Schmid factor. These low-rank SF twins have been referred to as "non-Schmid" twins. Activation of non-Schmid twins has also been reported in other HCP metal systems, like HCP Ti and AZ31 Mg alloy (Bieler et al. 2014; Kumar et al. 2018; Shi et al. 2015a, b; Wang et al. 2013c).

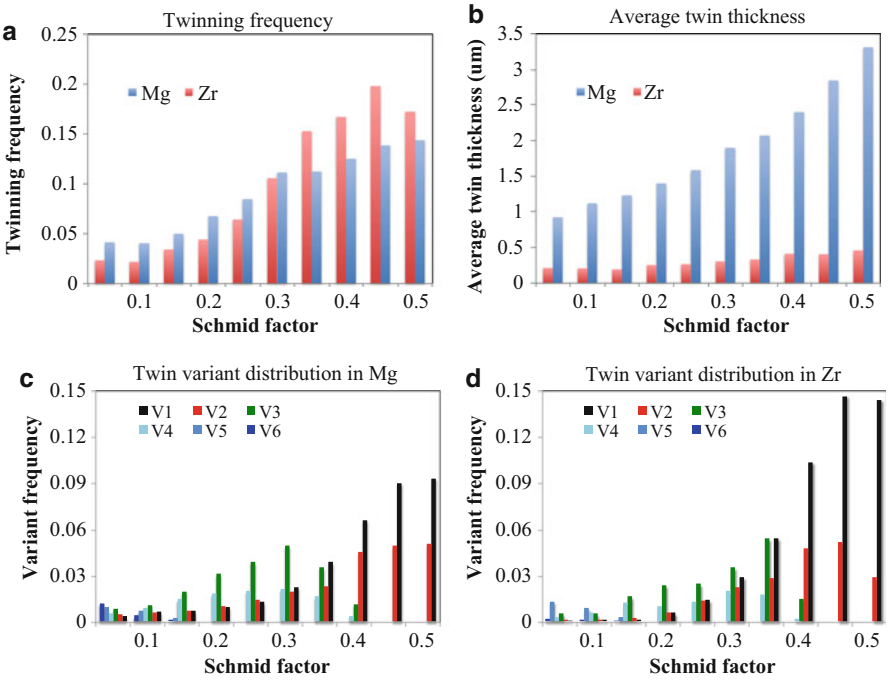

Fig. 4 Effect of grain orientation, as measured by the Schmid factor associated with the twin system, on (**a**) twinning frequency and (**b**) average twin thickness of $\{10\bar{1}2\}$ tensile twins in deformed Mg (Beyerlein et al. 2010) and deformed Zr (Capolungo et al. 2009). (**c**) and (**d**) are the corresponding twin variant distributions in Mg and Zr, respectively

With all else being the same, twins with high geometric SF are expected to be thicker compared to twins with low SF. From the statistical data set, Fig. 4b shows the distribution of twin thickness as a function of SF for Mg and Zr. Evidently, twins with higher SF are thicker, presumably because they are better oriented for growth.

2.4 Statistical Analysis of Grain Size Effects

A common finding in many metals, not only those of HCP crystal structure, is that polycrystals with smaller average grain sizes develop lower twin volume fractions (Barnett et al. 2004, 2012; Beyerlein et al. 2010; Capolungo et al. 2009; Ecob and Ralph 1983; Ghaderi and Barnett 2011; Gutierrez-Urrutia and Raabe 2012; Jain et al. 2008; Juan et al. 2015; Kang et al. 2016; Kumar et al. 2016c, 2018; Lentz et al. 2014; Liu et al. 2015; Rahman et al. 2015; Stanford and Barnett 2008; Tsai and Chang 2013; Wongwiwat and Murr 1978). This frequent observation has motived the application of the Hall-Petch scaling law, originally used for slip, to twinning. This law was first used to explain the higher yield stresses or fracture strains with

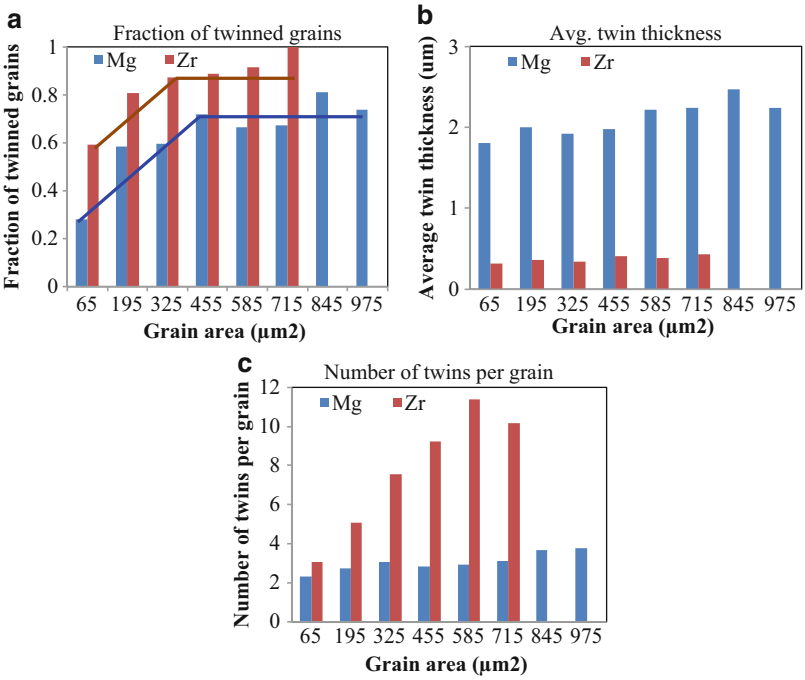

Fig. 5 Effect of grain size on (**a**) twinning frequency, (**b**) average twin thickness and (**c**) average number of twins per twinned grain of $\{10\bar{1}2\}$ tensile twins in Mg (Beyerlein et al. 2010) and Zr (Capolungo et al. 2009)

decreasing grain size. For twinning, it has been applied in a similar way, such as a twinning stress that increases according $1/\sqrt{D}$, where D is grain size. In nearly all of these cases, the grain size refers to the diameter of the grain that has been cut in the 2D scan. In this section, the grain size dependence on twin frequency from statistically large EBSD data sets are discussed.

The variation in twinning tendency (defined as the number of twinned grains/total number of grains) with grain size for Mg and Zr is shown in Fig. 5a. Here the twinned grains refer to grains with at least one twin of any type. The analysis finds that for both material systems, the propensity for twin activation increases with increasing grain size. It is worth noting that the grain size dependence is not monotonic: the grain size dependence is more pronounced for smaller size grains and tends to saturate for larger grains (see Fig. 5a). The distribution of average twin thickness as a function of grain size is shown in Fig. 5b. The grain size plays a strong role on twin thickness in Mg, but not so in Zr. As another twinning metric, Fig. 5c shows the effect of grain size on the formation of multiple twins in HCP Mg and Zr. In both the materials, the number of twins per grain increases with increasing grain size, but it is particularly striking in Zr. Taking all the data into account, it appears that a grain of a given size in Zr accommodates more twins than grains of the same

size in Mg. Similar twinning statistics has been studied in other HCP metals and for other types of twins (Ghaderi and Barnett 2011; Juan et al. 2015; Lentz et al. 2015, 2016).

3 Computational Modeling Methods

3.1 Challenges in Modeling the Stochastic Twinning Process

In the foregoing section, statistical aspects of deformation twins were discussed. The substantial spatial variability in these features, across a deformed material grain structure, presents challenges in building both understanding and material models for several reasons. Firstly, twins appear to form randomly as the material is being deformed, and the origins of this stochastic behavior still need to be fully understood. Secondly, the discrete nature of twinning makes it inherently inhomogeneous, making the more commonly used and computationally efficient homogenization mean-field models not readily applicable to treat materials that undergo profuse deformation twinning. Thirdly, twin development is naturally a multiscale process. Twins initiate at the atomic scale, form embryos at the nanoscale, and grow to the submicron scale and can propagate across a grain and grain structure, manifesting at the micron scale and larger. Thus, it is not readily apparent how to apply coarse-graining modeling techniques to deformation twinning. Last, twins do not occur in isolation but concurrently with slip. The shear for HCP metals for the most common $\{10\bar{1}2\}$ tensile twin is 13% for Mg. Thus, even if the entire grain were to twin, slip would need to occur simultaneously in order to plastically strain the material. Twin-slip interactions are just as important or arguably more important for understanding the constitutive response of a material that deforms by slip and twinning. These interactions cannot be fully understood by studying slip and twinning separately.

3.2 Some Important Components for Models of Polycrystalline Materials That Deform by Slip and Twinning

Modeling the deformation of polycrystalline materials has been accomplished via a combination of crystal plasticity theory and polycrystal modeling schemes. Crystal plasticity (CP) theory is used to relate the distortion of a strained crystal to slip on crystallographic slip systems (Asaro 1983; Asaro and Lubarda 2006; Hosford 1993). Polycrystal plasticity models then link the individual grain response predicted by CP theory to the overall mechanical response of the polycrystalline aggregate (Asaro 1983; Canova et al. 1988; Kocks 1970; Kocks et al. 2000; Peirce et al. 1982; Roters et al. 2010; Tome et al. 1984). These polycrystal models appear in various levels of sophistication and computational efficiency as will be discussed shortly.

Implementing deformation twinning into a polycrystalline model would ideally seek to include the following elements: (1) the available twin modes, (2) a model

for activating a twin or a number of twins inside a grain, (3) a criterion for variant selection of the activated twins, (4) a scheme for reorienting and shearing the portion of the grain that is twinned, and (5) a criterion to grow the twin. Additional elements include accounting for twin-slip interactions and twin-twin interactions and twin transmission across grains. Not as many models exist that account for these other phenomena, in spite of the fact that they are common occurrences.

3.3 Two Categories of Computational Methods for Modeling Twins in Polycrystals

Computational crystal plasticity-based material models for the deformation of polycrystalline materials can generally be broken down into two categories: mean-field models and full-field, spatially resolved models. The homogenized or mean-field response models, such as self-consistent models, take only a statistical description of the microstructure as input (e.g., crystallographic texture) and return a sample scale or effective response and microstructure evolution (Kocks et al. 2000). In this chapter, the visco-plastic self-consistent (VPSC) model is presented as an example for homogenized models (Lebensohn and Tome 1993).

Full-field micromechanical models, such as crystal plasticity finite element (CPFEM)- or crystal plasticity fast Fourier transform (CPFFT)-based approaches, require as input an explicit spatially resolved description of the material structure (e.g., grain orientation map) and return the spatially resolved material response and local structural evolution (Abdolvand and Daymond 2013b; Abdolvand et al. 2011; Ardeljan et al. 2016; Bronkhorst et al. 1992; Delannay et al. 2006; Eisenlohr et al. 2013; Idiart et al. 2006; Kalidindi 1998; Kanjarla et al. 2012b; Knezevic et al. 2016; Lebensohn 2001; Lebensohn et al. 2008, 2011a, b, 2012; Liu et al. 2010; Masson et al. 2000; Michel et al. 2000, 2001; Mika and Dawson 1999; Moulinec and Suquet 1994, 1998; Shanthraj et al. 2015; Zecevic and Knezevic 2017; Zhao et al. 2007). The term "full-field" indicates that both long-range and short-range grain interactions are considered, and the micromechanical fields are resolved on a discrete grid.

3.4 Homogenized VPSC Model Framework

VPSC model describes the polycrystal as a collection of orientations (grains) each with associated volume fraction. Each grain is regarded as a visco-plastic inclusion embedded in, and interacting with, a "homogeneous effective medium" (HEM), which has the average properties of the polycrystalline aggregate. The macroscopic response of the polycrystal results from the contribution of each grain. The visco-plastic compliance of the HEM is given by a self-consistent condition applied on the grain averages. At the single crystal level, the strain rate is given by the individual shear contributions of all active slip and twinning systems in the grain, as:

$$\dot{\varepsilon}_{ij}^{g} = \sum_{s} m_{ij}^{s} \dot{\gamma}^{s} = \dot{\gamma}_0 \sum_{s} m_{ij}^{s} \left(\frac{m_{kl}^{s} \sigma_{kl}^{g}}{\tau^{s}} \right)^{n} \tag{1}$$

Here, $\boldsymbol{m}^s$ is the symmetric Schmid tensor and $\dot{\gamma}^s$ is the shear rate on system s, $\dot{\gamma}_0$ is a normalized shear rate, n is the inverse strain-rate sensitivity, and τ^s is the threshold or critical resolved shear stress required to activate system s. The latter is evolved using a thermally activated dislocation density-based hardening law (Beyerlein and Tome 2008). In order to avoid the further strain-rate dependence associated with the power n in Eq. (1), $\dot{\gamma}_0$ is chosen equal to the norm of the macroscopic strain rate $\left\| \overline{\dot{\varepsilon}}_{ij} \right\|$. The constitutive laws relating strain-rate and stress for a single crystal and for the aggregate are written in a linearized form as:

$$\begin{aligned} \dot{\varepsilon}^{g} &= M^{g} : \sigma^{g} + \dot{\varepsilon}_0^{g} \\ \overline{\dot{\varepsilon}} &= \overline{M} : \overline{\sigma} + \overline{\dot{\varepsilon}}_0 \end{aligned} \tag{2}$$

where M^g and $\overline{M}$ are the grain and the macroscopic visco-plastic compliance tensors. The tensors $\dot{\varepsilon}_0^g$ and $\overline{\dot{\varepsilon}}_0$ are the back-extrapolated terms for the grain and aggregate, respectively. These variables result from the linearization of Eq. (1). The effect of the linearization scheme on individual grain and polycrystal responses, thus, emerges only through these two variables.

The inclusion formalism couples stress and strain-rate in the grain $(\sigma^g, \dot{\varepsilon}^g)$ with the average stress and strain-rate in the effective medium $\left(\overline{\sigma}, \overline{\dot{\varepsilon}}\right)$ through an interaction equation:

$$\left(\dot{\varepsilon}^{g} - \overline{\dot{\varepsilon}}\right) = -\tilde{M} : \left(\sigma^{g} - \overline{\sigma}\right) \tag{3}$$

where

$$\tilde{M} = n^{\text{eff}} (I - E)^{-1} : E : \overline{M}^{\text{secant}} \tag{4}$$

and E is the visco-plastic Eshelby tensor, $\overline{M}^{\text{secant}}$ is the macroscopic visco-plastic compliance tensor for the secant interaction $\left(\overline{\dot{\varepsilon}}_0 = 0\right)$, and the parameter n^{eff} "tunes" the stiffness of the inclusion-matrix interaction: $n^{\text{eff}} = 0$ for a Taylor case and $n^{\text{eff}} = 1$ for the stiff secant case.

3.5 Twinning in SC Approach: CG Model

An aspect of twinning that needs to be incorporated into the models is the fact that twins are finite domains that reorient the lattice and shear portions of the grain (usually taking on a lamellar morphology) and introduce a twin boundary. Over the years, a number of methods have been introduced for treating the

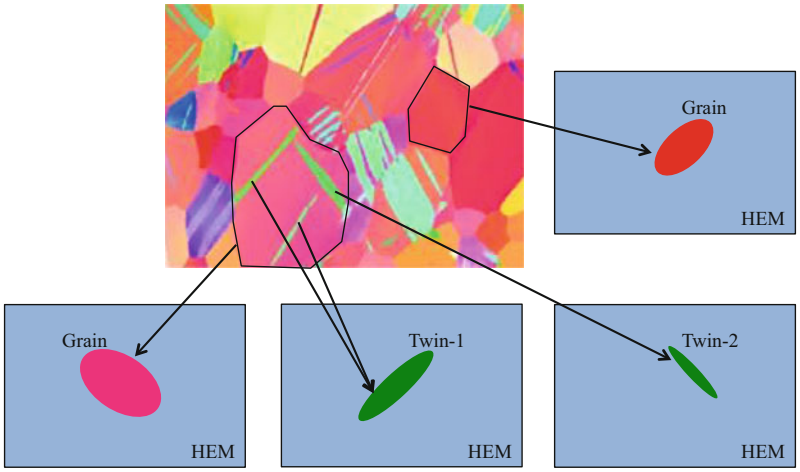

Fig. 6 Schematic of the composite-grain (CG) model for modeling twin reorientations within the VPSC framework. Un-twinned grain is represented as an ellipsoidal inclusion within a homogenous effective medium (HEM). For twinned grains, which may be comprised of one twin variant type or multiple variants, the matrix and each twin variant is represented as separate inclusions. As an example, "Twin-1" corresponds to two twins of the same variant, and "Twin-2" corresponds to another twin variant, all within the same grain. Here the HEM represents the average response of the polycrystal except the chosen grain and/or twin

reorientation that accompanies twinning: (i) predominant twin reorientation (PTR) method (Lebensohn and Tome 1993; Tome et al. 1991) and composite-grain (CG) method (Proust et al. 2009; Proust et al. 2007), for instance. In these schemes, the twin phase replaces some fraction of the matrix phase, and as the volume of the twin phase increases with strain, the volume of the matrix phase shrinks accordingly. They generally involve splitting the original orientation (grain) into two parts, one part that is twinned and another part that is the matrix, while preserving the original volume fraction of the grain. For instance, in the CG method, the newly twinned grain is split into two inclusions, a twin inclusion with the twinned volume fraction and the remaining parent inclusion with the remaining fraction. The newly formed twin inclusions are treated as new ellipsoidal inclusions and added to the total number of grains in the polycrystal. As grains in these models are represented as ellipsoidal inclusions, the new twin inclusions can be made initially flat ellipsoids with their short axis perpendicular to the twinning plane, to reflect the lamellar shape of newly formed twins (see Fig. 6). The twinned inclusion adopts a mirror orientation with respect to the orientation of the parent grain, that is, characteristic of the type of twin (Yoo 1981; Yoo and Lee 1991).

Later, a modified CG model was developed, which allows for multiple twin types and variants to form in the same grain (Niezgoda et al. 2014). In the modified CG model, the twin and matrix grains are treated as two noninteracting inclusions (grains) embedded in the homogeneous effective medium. It is schematically shown

in Fig. 6. In the figure, a grain with two types of twin variants is shown, and in this case, un-twinned matrix grain, twin of variant 1, and twin of variant 2 are considered separate inclusions in the effective medium. The two twins are initially given a flat ellipsoid shape. The shortest axis of the ellipsoid is parallel to the twinning plane normal and another of the ellipsoid axes is parallel to the twinning direction. A similarly oriented ellipsoid is created to represent the un-twinned region of the grain. The aspect ratios of both ellipsoids evolve with deformation. These twin and matrix grains are characterized by independent secant compliances M^{sec}, and consequently no explicit twin-matrix interaction is considered when solving the self-consistent equations. The relative fraction of each phase is updated incrementally with deformation as the grain twins.

Once a twin has formed inside a grain, growth of this twin is determined in a more traditional deterministic fashion within the modified CG framework. During deformation, the twin shear rate $\dot{\gamma}^{v}$ is calculated for the nucleated twin or variant v in each grain by:

$$\dot{\gamma}^{v} = \dot{\gamma}_0 \left(\frac{\tau^{v}}{\tau_c^{twin}} \right)^{n} \tag{5}$$

Here τ^{v} and τ_c^{twin} are the resolved shear stress on twin variant v, and critical resolved shear stress for twin domain expansion (after nucleation).

3.6 Full-Field CPFFT Model Framework

The FFT-based crystal plasticity-based models provide spatially resolved micromechanical fields in the individual crystals within polycrystals. The formulation provides an exact solution of the governing equations of equilibrium and compatibility, in such a way that the final (converged) equilibrated stress and compatible strain fields fulfill the constitutive relationship at every discrete material point.

The original FFT formulation was developed to study the local and effective mechanical response of linear elastic (Moulinec and Suquet 1994), nonlinear elastoplastic (Moulinec and Suquet 1994, 1998), and visco-plastic (Michel et al. 2000, 2001) composite materials. The FFT formulation was later adapted for polycrystalline materials and permitted the study of the effective and local responses associated with the heterogeneity in the spatial distribution of crystallography and directional dependence of mechanical properties (Lebensohn 2001). In recent years, this FFT formulation has been extended to different deformation regimes like elasticity (Brenner et al. 2009), incompressible visco-plasticity (Lebensohn 2001; Lebensohn et al. 2008), dilatational visco-plasticity (Lebensohn et al. 2011b), infinitesimal elasto-visco-plasticity (Kanjarla et al. 2012b; Lebensohn et al. 2012) and finite elasto-visco-plasticity (Eisenlohr et al. 2013). Below the CPFFT model that allows for the crystals to deform by infinitesimal elasto-visco-plasticity (EVP)

is briefly described and applied in later examples to study stress fluctuations in a deformed polycrystal and local stress states generated around discrete twins.

In the CPFFT method, the solution of an EVP problem involves the adoption of an appropriate time discretization scheme. Using an Euler implicit time discretization and Hooke's law, the expression for the stress in material point x at $t + \Delta t$ is given by:

$$\boldsymbol{\sigma}^{t+\Delta t}(x) = \mathbf{C}(x) : \boldsymbol{\varepsilon}^{e,t+\Delta t}(x) = \mathbf{C}(x) : \left(\boldsymbol{\varepsilon}^{t+\Delta t}(x) - \boldsymbol{\varepsilon}^{p,t}(x) - \dot{\boldsymbol{\varepsilon}}^{p,t+\Delta t}(x)\,\Delta t\right) \tag{6}$$

where $\sigma(x)$ is the Cauchy stress tensor; $C(x)$ is the elastic stiffness tensor; $\varepsilon(x)$, $\varepsilon^e(x)$, and $\varepsilon^p(x)$ are the total, elastic, and plastic strain tensors; and $\dot{\varepsilon}^p(x)$ is the plastic strain-rate tensor given in Eq. (1). The CPFFT model solves the equilibrium equation along with the above constitutive equation by iteratively adjusting the compatible strain field at every material point. The spatially resolved local response is calculated using the convolution integral between the Green's function associated with the displacement field of a linear reference homogeneous medium and a polarization field in which the heterogeneity and nonlinearity of the problem is specified. Application of Fourier transforms reduces the convolution integrals of the equilibrium equation in real space into simple products in Fourier space. Specifically the FFT algorithm transforms the polarization fields of the periodic microstructures, which are functions of the unknown strain field, into Fourier space, to obtain the micromechanical responses in real space.

3.7 Twinning Model in CPFFT Framework

Up to now, advancing CP models for discrete twins with a 3D microstructure has been hindered by the lack of 3D microstructural representation codes. Very recently, a few full-field, spatially resolved polycrystal models, such as CPFFT and CPFEM, have been advanced to include discrete twin domains within individual grains (Abdolvand and Daymond 2013a, b; Abdolvand et al. 2011, 2015b; Abdolvand and Wilkinson 2016; Ardeljan et al. 2015). To model the twin domain, the boundary of the domain, the twinning orientation, and the characteristic twin shear needs to be imposed homogeneously throughout the domain. A few examples of the local stress fields calculated around twins in Zr and uranium (U) with these techniques are shown in Fig. 7 (Abdolvand and Wilkinson 2016; Ardeljan et al. 2015). An important aspect captured is the heterogeneous stress field within crystals that result from the twin. The character, intensity, and extent of these fields depend sensitively on the elastic and plastic properties of the material. Recently a series of studies were undertaken to understand how response of the surrounding crystal could impact the mesoscopic processes of twinning (Abdolvand et al. 2018; Kumar et al. 2015, 2016a, b, c, 2017b).

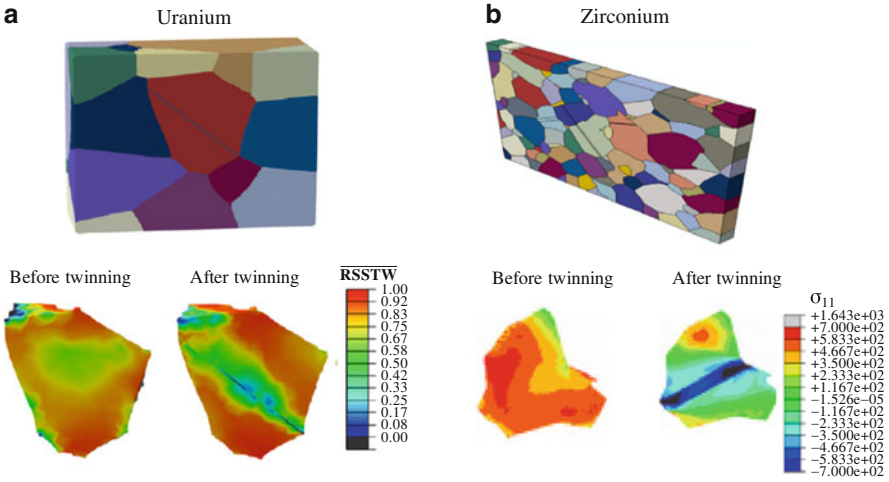

Fig. 7 Examples of recent modeling efforts in which discrete twin lamellae have been included within a full-field spatially resolved technique. The two shown are crystal plasticity finite element (CPFEM) models for (**a**) uranium (Ardeljan et al. 2015) and (**b**) zirconium (Abdolvand and Wilkinson 2016)

In this section, the recent extension of the CPFFT formulation to account for the reorientation and twinning shear transformation in discrete regions within a crystal is described. In this model, deformation twinning is treated as a shear transformation process. Accordingly the constitutive behavior of an elastic-visco-plastic material under an infinitesimal strain approximation with shear transformation becomes:

$$\boldsymbol{\sigma}^{t+\Delta t}(x) = \mathbf{C}(x) : \left(\boldsymbol{\varepsilon}^{t+\Delta t}(x) - \boldsymbol{\varepsilon}^{p,t}(x) - \dot{\boldsymbol{\varepsilon}}^{p,t+\Delta t}(x)\,\Delta t - \boldsymbol{\varepsilon}^{tr,t}(x) - \Delta\boldsymbol{\varepsilon}^{tr,t+\Delta t}(x)\right) \tag{7}$$

where $\boldsymbol{\varepsilon}^{tr}$ is the transformation strain. During the buildup of the twinning transformation, successive shear increments are imposed in the twin domain and the system relaxed. The associated strain increments have the following relationship with the local twin variant at point x:

$$\Delta\boldsymbol{\varepsilon}^{tr}(x) = \mathbf{m}^{tw}(x)\,\Delta\gamma^{tw}(x) \tag{8}$$

For material points lying outside the twin domain, $\Delta\varepsilon^{tr}(x)$ is zero. The tensor $\mathbf{m}^{tw} = \frac{1}{2}\left(\mathbf{b}^{tw} \otimes \mathbf{n}^{tw} + \mathbf{n}^{tw} \otimes \mathbf{b}^{tw}\right)$ is the Schmid tensor associated with the twinning system, where $\mathbf{b}^{tw}$ and $\mathbf{n}^{tw}$ are unit vectors along the twinning direction and twin plane normal, respectively. The twinning transformation builds up in increments, until reaching the characteristic twin shear, s^{tw}:

$$\Delta\gamma^{tw}(x) = \frac{s^{tw}}{N^{twincr}} \tag{9}$$

The time increment Δt and the number of increments to achieve the twin transformation N^{twincr} are set sufficiently low and high, respectively, to ensure convergence.

4 Stochastic Twin Nucleation Model

4.1 Probability Model for Critical Stresses for Twin Formation

In a few recent works (Beyerlein et al. 2011; Beyerlein and Tome 2010; Niezgoda et al. 2014), an approach was developed to include grain boundary-induced twin nucleation into constitutive laws for application into the mean-field crystal plasticity models, like VPSC with a twin reorientation scheme. Unlike conventional polycrystal models to date, the model they used for twin nucleation is not deterministic but probabilistic, dictated by the likelihood of forming a twin embryo in the grain boundaries. The approach involves incorporating two aspects of the grain boundaries in a bulk average probabilistic sense. One aspect is a probability model for the nucleation of twins when some numbers of grain boundary defects undergo stress-driven transformations, which then coalesce into a single stable nucleus. It assumes that the time scale of the transformation and subsequent coalescence is instantaneous compared to the applied deformation and introduces a characteristic length scale, within which a critical number of transformations occur to produce a propagating twin. The stochastic model gives an explicit form for the probability distribution for the critical stress values required for twin nucleation that could be used in the VPSC model for activating twinning.

The other aspect concerns the stresses that activate twinning. These stresses are those that are generated at grain boundaries, and these tend to deviate significantly from the average stresses calculated in VPSC for each grain. To tackle this, distributions of grain boundary stresses were obtained from separate full-field CP calculations. Taken together the VPSC model simulations of deformation were advanced to activate twinning when randomly sampled critical twin stresses were exceeded by randomly sampled grain boundary stresses.

In this section, the model is briefly reviewed. Consider a grain within a polycrystal as illustrated in Fig. 8. It has n_f nearest neighbors and is joined to each neighbor k ($k = 1, \ldots n_f$) by a common grain boundary facet of area A_k. Connecting these facets is a network of triple lines and quadruple points, which generally have an atomic structure distinct from those of the facets.

A grain boundary area A_k contains defects, or grain boundary dislocations (GBDs), varying spatially and temporally in defect content (e.g., size of the Burgers vector). When provided a sufficiently high stress for a GBD of a given size, GBDs can transform into a twin embryo, a process observed in atomistic simulation to involve the reshuffling of the atoms into the twinned structure (Wang et al. 2013b).

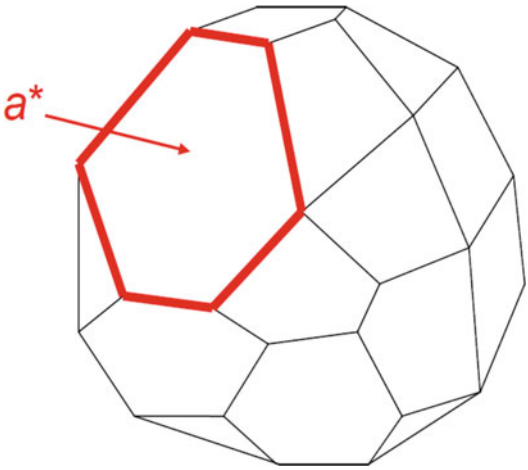

Fig. 8 Illustration of a grain in a polycrystal with the neighboring grains not shown (Beyerlein and Tome 2010). The boundary of the grain is comprised of a network of facets (with area a*), triple lines, and quadruple points

Neighboring smaller twin nuclei can coalesce into a larger twin embryo. If the embryo reaches a critical size, it will propagate into the crystal (Beyerlein and Tome 2010).

According to this physical picture, forming an embryonic twin relies on the right stress fluctuation simultaneously hitting the right-sized defect. This confluence of events is more likely to occur in the grain boundaries, where local stress states and defect content are high. It is usually the case that the spatial distribution of GBDs and stresses are heterogeneous, a GBD-to-twin nucleus transformation is a statistically occurring event, and the number of such events N is a random variable. The number N is expected to increase as the area A_k of the facet and the magnitude of the stresses acting on the boundary increase.

In the model, a stochastic counting process is proposed for N, i.e., $\{N(A_k), A_k \geq 0\}$, where $N(A_k)$ is the number of transformation events that occurred in an area A_k. If each event is independent and identically distributed (i.i.d.), and the number of events in nonoverlapping elements is independent (stationary increments), then the Poisson process emerges as an appropriate model. Accordingly, the probability that $N = m$ defects will be transformed into a twin nucleus within a given area $A_k = a$ follows a Poisson distribution:

$$P\,(N = m, a) = \frac{(\lambda a)^m}{m!} \exp\,(-\lambda a) \tag{10}$$

where λ is the rate of the process. The parameter λ also corresponds to the expected number of transformation events per unit area. Another consequence of the Poisson model is that the events are uniformly distributed over area a, and spatial separation between transformation events is exponentially distributed. As the process is driven by stress, the Poisson rate λ is assumed a monotonically increasing function of the

resolved shear stress (τ) on a twin system s. For convenience, the following power law formulation is introduced:

$$\lambda(\tau) = \frac{1}{a_0}\left(\frac{\tau}{\tau_0}\right)^{\alpha} \tag{11}$$

where a_0 is a material parameter assumed to be constant, and τ_0 is a characteristic scalar stress value, which is interpreted as the stress required to dissociate, on average, one grain boundary dislocation on area a_0. Parameters a_0 and τ_0 are, in principle, functions of the defect content of the grain boundary. Therefore, they may vary from boundary to boundary and differ, for instance, for a coherent boundary versus an incoherent one.

To implement the above model into a computational mechanics code, the discrete counting of the number of transformation events needs to be linked to a continuous probability of forming a twin nucleus. To this end, a characteristic area a_c is introduced as the minimum area that can produce one twin, i.e., one characteristic area a_c produces one crystalline twin, which may have resulted from the coalescence of n tinier twin nuclei created by n transformation events. Suppose that at least m^* distinct conversion events need to occur within a_c in order to form one twin, then the probability that at least m^* events occur in a_c is:

$$P\left(N \geq m^*, a_c\right) = 1 - \sum_{m=1}^{m*-1} P(N = m, a_c) \tag{12}$$

Further, we assume that $m^* = 1$, that is, at least one defect must be activated within a_c, which yields the following Weibull distribution.

$$P(S < \tau) = P(N \geq 1, a_c) = 1 - \exp\left(-\left(\frac{\tau}{\tau_c}\right)^{\alpha}\right) \tag{13}$$

Using Eqs. (12) and (13), we can redefine $P(S < \tau)$ as the probability that the critical stress to nucleate a twin is less than or equal to τ. Here S is a random variable that quantifies the critical nucleation strength or equivalently the stress required to transform an appropriate number of grain boundary dislocations into twinning dislocations.

The area a_c is an important model length scale, where in all dissociation events in a_c lead to one twin. Accordingly, it sets the minimum twin spacing and the maximum number of twin lamellae that can form from a grain boundary of area A_k as $n^* = A_k/a_c$. The material parameter α governs the dispersion in S and is linked to the type of defects in the grain boundary.

4.2 Statistical Representations of Grain Structures

The above model applies to twinning from one-grain boundary facet of area A_k. Multiple grain neighbors in fact surround any given grain, and each neighbor shares just one of the many facets that comprise a grain's boundary.

Recall from Sect. 4.1 that in a given grain facet A_k, there are n^* number of potential sites to form a twin. Correspondingly, following Eq. (13), there is a set of n^* critical stresses S_i, $i = 1, \ldots n^*$, assumed to be independent and identically distributed. In order to assign the number of potential nucleation sites n^* for each grain, the three-dimensional grain structure is needed. At a minimum, the microstructural parameters needed are (1) the number of neighbors (n_k) or number of grain boundary facets of a grain and (2) the surface area of the grain boundary facets A_k from which the twins will nucleate. These parameters depend on the grain size distribution and the morphology of the grains in the sample and can in principle be estimated from a combination of microscopy and some basic stereological principles.

When the computational model is a mean-field model, like VPSC, every grain is modeled as an ellipsoidal inclusion. Thus estimates are needed for the lattice orientation, effective radius (or equivalently volume), and the ratio between major and minor axes of the grains. For this purpose, the stochastic field model of Thorvaldsen (1993) is adopted. Using simple geometric arguments, this model develops an expression for the distribution of neighbors for a given grain and the distribution of facet areas depending on its size, R, and shape. According to this model, for a spherical grain with radius R, the expected number of grain neighbors n_f, $E(n_f)$, is related to the expected value of R, E(R) according to:

$$E(n_f) = 4\left(1 + \frac{R}{E(R)}\right)^2 \tag{14}$$

Given a neighboring grain with radius R_n, the contact area, A_k, is given by (Thorvaldsen 1993):

$$\frac{1}{A_k} = \frac{1}{\pi}\left(\frac{1}{R_n} + \frac{1}{R}\right)^2 \tag{15}$$

To demonstrate, the mode is applied to high-purity HCP Zr. Figure 9 shows the distribution of grain size (Capolungo et al. 2009), the predicted distribution for the number of neighboring grains or facets, and the predicted distribution of grain facet areas for Zr. The equivalent circle radius exhibits an approximate Rayleigh distribution. Accordingly, the cross-sectional grain areas will be exponentially distributed. The expected number of neighbors for this grain size distribution is 17, indicating a wide range of grain sizes in the Zr aggregate being modeled.

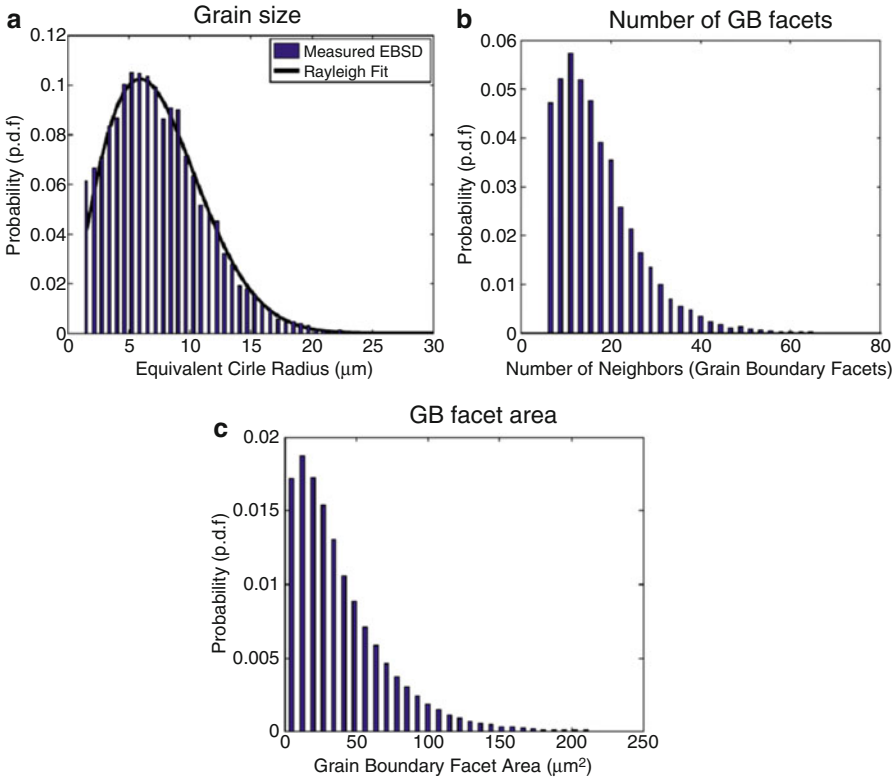

Fig. 9 Microstructural variations considered in the stochastic twin nucleation model: (**a**) grain size, (**b**) number of grain boundary facets, and (**c**) grain boundary facet area (Niezgoda et al. 2014). These microstructural distributions are obtained from the EBSD-based statistical analysis of pure Zr (Capolungo et al. 2009)

4.3 Spatially Resolved Stress States in Deforming 3D Polycrystals

This critical stress τ_c can then be compared to the twin-plane resolved shear stress (TRSS) for the twin variant in question. If it exceeds the TRSS, then a twin embryo may nucleate, and if not, then the region remains un-twinned. For twinning, the local stress state in the region in question for twinning is desired. Self-consistent schemes can be used to calculate the local stress state in the grain. However the formulation does not allow for calculation of the stress state in the boundaries. Also by modeling each grain as an ellipsoid in a homogeneous medium, the scheme does not provide a way of defining the orientation of the grain boundary with respect to the loading direction. Full-field, spatially resolved techniques such as CPFFT or CPFE, however, are particularly well suited for calculating stress distributions within grains and in grain boundaries and triple and quadruple points. From this

model, the stress fluctuation distributions, the deviation in stress from the average value, can be calculated and amenable for use in a mean-field technique.

Following this approach, CPFFT calculations are carried out on Zr. Several (100) realizations of 3D grain structures of representative Zr material volumes were performed to extract the stress fluctuations at grain boundaries (Kanjarla et al. 2012a; Niezgoda et al. 2013). The three-dimensional (3D) representative volume elements, RVEs, were created using DREAM-3D. Each RVE contained 500 ± 50 grains with ~5 × 10^5 grain boundary voxels or elements per RVE. For each representative volume, simulations of multiple loading conditions were performed. The deviations from the grain-averaged stress at the grain boundaries were extracted for all representative volumes for each loading condition.

For one example RVE, Fig. 10a shows calculated stress fluctuations, defined as deviations in the Von-Mises effective stress from the grain average stress, at 2.5% applied strain. This result reveals significant deviations at the grain boundaries. It is not uncommon for single grains to have regions near their boundaries that deviate in both a highly compressive and tensile state from the grain average. Figure 10b presents the observed deviations in the normal stress components from the grain stress. By averaging over multiple loading conditions, the fluctuations on all three normal components had approximately the same distribution, as did the three shear stress components. As shown, the distributions are approximately Gaussian; however, the extreme tails of the distributions extend significantly farther than would be expected from a perfect Gaussian. For VPSC deformation simulations, a six-dimensional Gaussian with a zero mean vector was used to reasonably represent the CPFFT calculations.

4.4 Incorporation of Statistical Stress and Strength Distributions in Homogenization Models

Carrying out the simulation with the probability model for twinning added, the VPSC model needs as input the distribution for the twin nucleation stresses and stress fluctuations. Figure 10c shows the former, the twin nucleation stress distribution for $a_c = 0.01\ \mu m^2$, $\alpha = 11.1$, and $\tau_c = 310$ MPa. The latter stress fluctuations, just described in the prior section, are provided in Fig. 10b. In an actual polycrystal, grain boundary misorientations are distributed, and their defect states vary, and in deformation, both can vary in time. However, for simplicity, the same Gaussian representation for the stress fluctuation distribution is applied for all grain boundaries at all times during deformation.

The procedure used is described as follows. The calculation begins with a description of the microstructure. The input texture for VPSC is constructed by sampling 8500 grains from the EBSD maps produced by Capolungo et al. (2009). The equivalent circle diameter from the EBSD is used to assign the weight or grain size for each grain (Fig. 9a). For each grain, Eq. (14) is used to determine the number of neighbors. The neighbors are randomly sampled from the input texture, and Eq. (15) is used to assign facet areas A_k. Each facet is then divided into n^* areas of

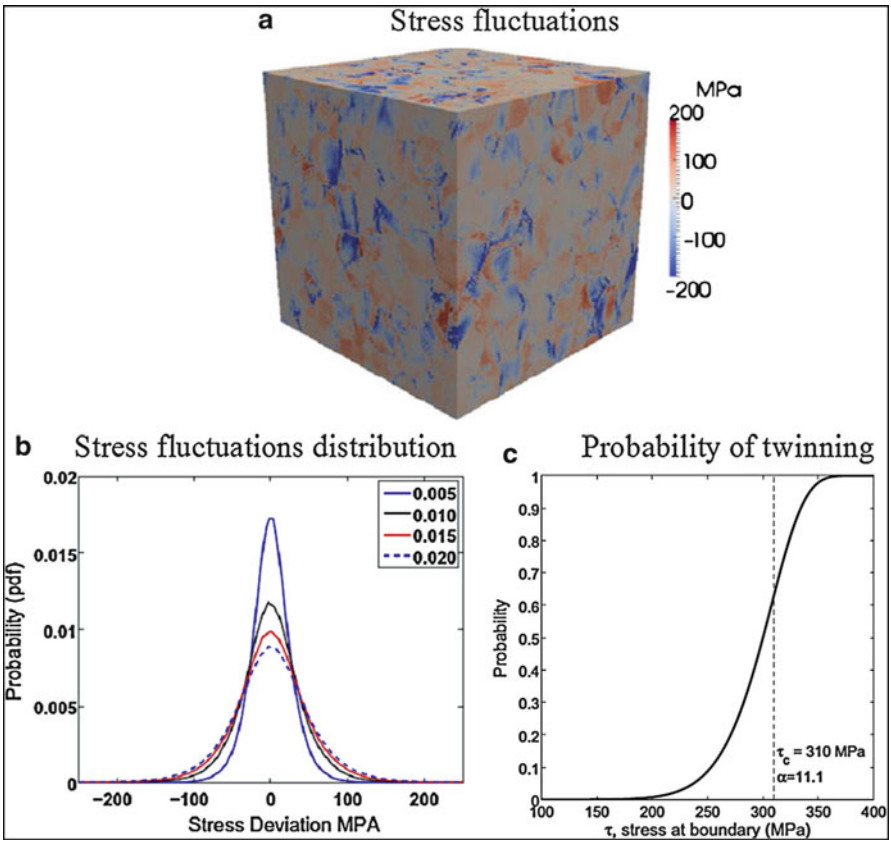

Fig. 10 Mechanical stress fluctuations as calculated in the CPFFT model: (**a**) the deviations in the effective stress from the grain average stress. The FFT model contains 522 grains (Niezgoda et al. 2013). (**b**) Distribution of the CPFFT calculated stress fluctuations from 100 different representative volume elements like those in (**a**) (Niezgoda et al. 2013). (**c**) Separately, the probabilistic nucleation model provides the probability distribution for the critical stress to form a twin (Niezgoda et al. 2014)

size a_c. Each of these areas is a potential nucleation site for a twin of variant v. For each site, at each strain increment, Eq. (13) is used to test for the nucleation of twin variant v, which requires knowing the resolved shear stress $\tau(v)$ projected on the twin variant v. To calculate $\tau(v)$, a stress fluctuation $\Delta\sigma$ is randomly sampled from the characteristic distribution (Fig. 10) for each variant and is added to the grain stress calculated at that strain increment. The sum is then projected onto the twin system to compute $\tau(v)$. This procedure for nucleation is then repeated for every twin variant at each site. In the case that multiple twin variants could nucleate from the same site, a single variant is selected at random to propagate. Each nucleation site is tested independently for nucleation, with no correlation with the neighboring sites. Although nucleation could occur on more than one facet belonging to a grain,

in these example calculations, one facet for each grain is randomly chosen as the one from which twins are allowed to grow. Using the above procedure, any variant could nucleate, not just the one with the highest $\tau(v)$. Once a grain forms twins, no further nucleation is allowed. Twin growth follows a deterministic stress-based criterion, Eq. (5).

Using the above model, the deformation response of HCP Zr at three different temperatures, liquid nitrogen (77 K), 150 K, and room temperature (300 K) is simulated. In this calculation plastic deformation of Zr is accommodated by prismatic <a> slip and pyramidal <c + a> slip and $\{10\bar{1}2\}$ tensile and $\{11\bar{2}2\}$ compression twins. The evolution of the critical resolved shear stresses for only the slip modes follows the dislocation density-based hardening model developed in Beyerlein and Tome (2008). The same twin nucleation stress distribution is used at all temperatures, while the effect of temperature is included in the initial CRSS and the dislocation density evolution rate for slip. Figure 11a compares the model-predicted stress-strain curves at 76 K, 150 K, and 300 K under in-plane compression with the experimental curves for Zr. As shown, good agreement in the calculated flow stresses and hardening rates for all temperatures tested is achieved. Although not shown, the model also predicts well the experimentally observed texture evolution (Fig. 6 of Niezgoda et al. 2014)) and twin volume fraction evolution (Fig. 8 of (Niezgoda et al. 2014)). For completeness, the calculated twin volume fraction at 5% and 10% compression for 76 K temperature loading is 4% and 16%, respectively, which agrees well with the measured fraction from EBSD images is 5% and 16%, respectively.

The importance of the stochastic twin nucleation model cannot be fully appreciated from analyzing average responses. The model results can also be compared to local, microstructure data distributions of twinning. Figure 11b compares the calculated number fraction of twins with a given Schmid factor after 10% compression at 76 K with the experimentally measured number distribution of the observed twins at the same strain from EBSD. Like the measurement, the calculated frequency is also broad, including twins with high Schmid factors and with low Schmid factors ($m < 0.3$). Figure 11c compares the model predicted frequency distribution of each twin variants with that from EBSD. The model finds that the twin variant selected is most likely (but not always) the one with the highest geometric Schmid factor and that the grains that twin are most often (but not always) well oriented for twinning, again, in agreement with the measurement. EBSD analysis indicates that only 50–60% of the twins correspond to the twin variant with the highest SF, i.e., v-1, and 20% to the second highest SF variant, v-2. Remaining ~20% of twins are the third and fourth highest SF variants.

The model overall predicts well the macroscopic deformation response because it predicts at the mesoscopic scale the formation of a broad range of twin variants over a broad straining period. In contrast, the model employing a deterministic twin nucleation approach, using a constant CRSS for all twins, predicts that ~95% of the twins activated are v-1 and the remaining ~5% are v-2. Lower ranked SF twin variants are not activated. The combined analysis of experiment and model results provides evidence that twin formation in polycrystalline materials is stochastic.

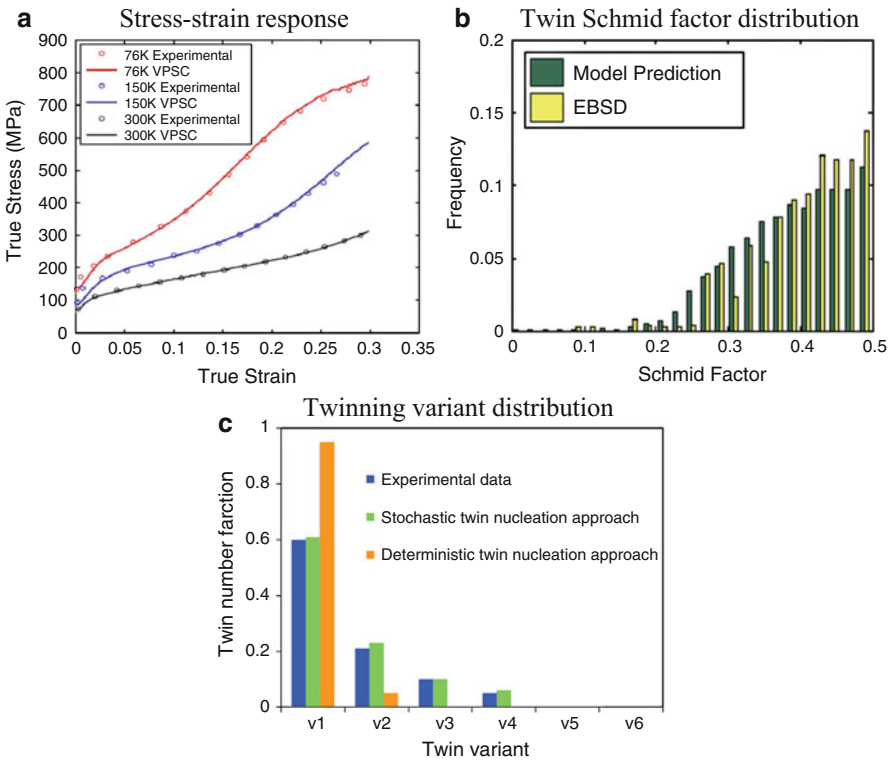

Fig. 11 Comparison of results from the VPSC model, with the twin nucleation model incorporated, for the (**a**) stress-strain response, (**b**) twinning frequency as a function of Schmid factor, and (**c**) twin number fraction for different twin variants at 10% compression. In (**c**), the frequency of twin variants formed as predicted from the polycrystal VPSC model with and without the stochastic twin model are compared. Without it, the criterion for forming a twin is deterministic. As shown, better agreement with the EBSD data is achieved with stochastic twin formation implemented (Niezgoda et al. 2014)

5 Stochastic Twin Growth Model

The earlier sections in this chapter discussed twin formation, as being derived from reactions involving intense localized stress and dissociations of individual or groups of discrete dislocations. The remaining sections of this chapter focus on the thickening of the twin band. In this stage, the dimensions of the twin domain lie above the atomic scale, being approximately submicron or micron and closer to the dimensions of the parent grain. The stress fields surrounding twin domains of this size range develop as a result of elastic and plastic deformation. The latter is carried by the collective glide of dislocations and can be adequately modeled at this scale by crystallographic slip. Accordingly, to study the effects of slip and crystal orientation on these two stages of deformation twinning, we employ a full-field,

spatially resolved technique, the CPFFT model, which permits calculation of the mechanical fields (stress, strain, strain rate) in the presence of discrete twin domains within crystals. In the examples that follow, the model is applied to $\{10\bar{1}2\}$ tensile twins in HCP Mg and Zr metals. The anisotropic elastic constants (in GPa) for Mg at room temperature are 59.75, 23.24, 21.70, 61.70, and 16.39 (Hearmon 1946; Simmons and Wang 1971) and for Zr at 77 K are 143.50, 72.50, 65.40, 164.90, and 32.10 (Fisher and Renken 1964; Simmons and Wang 1971). Plastic deformation is accommodated by basal <a>, prismatic <a>, and pyramidal <c + a> slip for both HCP Mg and Zr metals. The critical resolved shear stress (CRSS) for basal, prismatic, and pyramidal slip systems (in MPa) are 3.3, 35.7, and 86.2, respectively, for Mg at room temperature (Beyerlein et al. 2011), and 700.0, 20.0, and 160.0, respectively, for Zr at 77 K (Knezevic et al. 2015).

5.1 Local Twin Boundary Stresses to Expand Twin

As mentioned earlier, twins most often nucleate at a grain boundary and propagate across the grain until they are stopped at the opposing grain boundary. They thicken further after having terminated at grain boundaries. Both the surrounding parent and neighboring grains deform in order to accommodate the shear strains resulting from the growing twin. To investigate the driving forces for twin growth, it is important to understand the local stresses generated around the twin band. To this end, consider a tri-crystal of three neighboring grains embedded in a polycrystal, as shown in Fig. 12. The central grain contains the deformation twin, which spans the width and intersects with the two neighboring crystals. The parent grain orientation is (0°,0°,0°), (Bunge convention), which corresponds to alignment of its c-axis with the Z-direction.

Using CPFFT model, the stress and elastic and plastic strain tensorial fields are calculated, and for analysis, the TRSS field is presented in Fig. 12b after twinning. In this example, the neighboring grain orientation is (0°, 30°,0°) and the material is Zr. The stress inside the twin domain and along the lateral sides of the twins is negative, and in the neighboring grains, it is positive. Note that before the twin was present, the stress state was nearly uniform in the crystal, but when the twin is present, the stress state remains homogeneous in the twin domain but has become nonuniform, particularly in the matrix region immediately bordering twin. For more details, the TRSS distribution along the twin after twinning is given in Fig. 12c. The TRSS along the lateral interface of the twin band is negative, signifying that the negative TRSS along the twin boundary acts in the anti-twinning direction and thus serves as a resistance to further twinning. More quantitatively, a *twin backstress* field can be defined as the difference in the TRSS before and after twinning. The backstress is highest in value at each end, where the twin shear and reaction from the neighboring grain is the greatest and decays toward the middle of the twin. The backstress is the least at the middle of the twin. To migrate the boundaries, the applied load would need to be increased further such that the local TRSS along

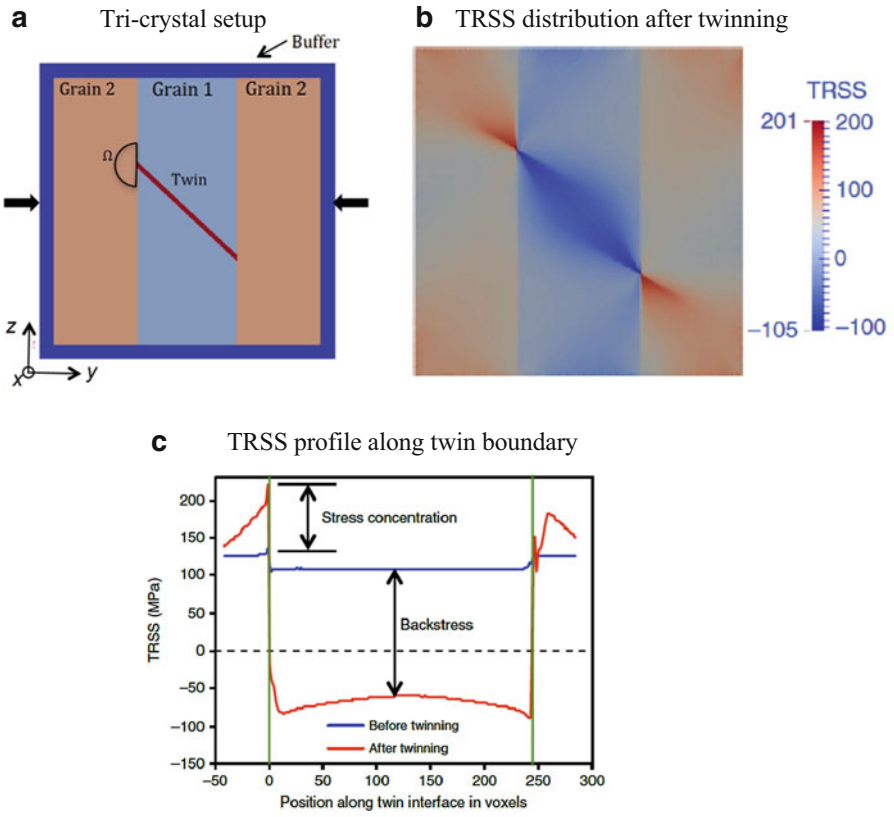

Fig. 12 CPFFT calculated twin stress distributions generated by a twin lamella in Zr (Kumar et al. 2016a). (**a**) Tri-crystal setup consisting of a central grain "grain-1" containing a twin and two neighboring grains, with the same orientation on each side. Orientations of grain-1 and grain-2 are (0°, 0°, 0°) and (0°,30°,0°), respectively. (**b**) The twin-plane resolved shear stress (TRSS) distribution after twinning and (**c**) TRSS profile along twin boundary before and after twinning

the twin becomes positive and exceeds a threshold value associated with boundary migration.

The amount of twin backstress observed here depends on the ability of the neighboring grain to accommodate the shear imposed by the twin. These grains deform elastically and plastically, and in the latter case, the plastic accommodation generally involves slip on multiple slip systems. For an HCP material, the activation barriers for slip depend on the mode of slip and typically include basal <a> slip, prismatic <a> slip, and pyramidal <c + a> slip. In the case of Mg, the easiest basal <a> slip (3 MPa) only provides two independent slip systems. Thus, basal slip alone would be insufficient to accommodate a general stress state, and in general the next easiest prismatic <a> slip and/or hardest pyramidal <c + a> slip would also have to be activated at the twin/grain boundary junction. A neighboring grain well oriented

to accommodate the shearing action of the twin mostly with its easy slip system would be considered a "plastically soft" neighbor. Less backstress would result in the twin domain, particularly along the twin boundary. In contrast, a neighboring grain that is oriented poorly for easy slip must activate relatively large amounts of the harder slip modes in order to accommodate the shearing of the twin. It would constitute a "plastically hard" neighbor. A higher backstress in the twin would result and more applied load would be required to grow the twin. The grain neighbor orientation effect could be one explanation for why in a polycrystal some grains twin and others do not, despite being of similar size and orientation (Beyerlein et al. 2010; Capolungo et al. 2009; Kumar et al. 2018).

5.2 Grain Neighborhood Effects on Stresses to Expand the Twin

In this section, we study the effect of neighboring grain orientation on the twin backstress and twin expansion. The EVP-FFT-based twinning simulations are performed for 221 different grain orientations that represent the entire orientation space of neighboring grains for a fixed parent grain orientation and twin type and variant. The neighboring grain orientation space is represented in the ϕ versus ϕ_1 plot, the two angles denoting the in-plane rotation and c-axis misorientation, respectively (Kumar et al. 2017b). Maps for Mg and Zr are given in Fig. 13a, b. The landscapes are very different for these two materials. The magnitudes and anisotropy in the backstress are much higher for Zr than Mg. In the case of Mg, the backstress is particularly low (∼22 MPa) for the neighboring grain when the c-axis misorientation ranges from 0° to ∼25° and from ∼65° to 90°, but slightly higher (∼25 MPa) for the c-axis misorientation range from ∼25° to ∼65°. In the case of Zr, the backstress is lower (∼75 MPa) for the c-axis misorientation range from 0° to ∼45° and substantially higher (∼105 MPa) for the c-axis misorientation range from ∼45° to 90°.

Whether a grain neighbor is plastically hard and non-accommodating, leading to a high backstress, or vice versa, plastically soft, leading to a low one depends on the crystal's ability to activate its easiest slip mode. For Zr, the easier modes are prismatic slip and tensile twinning, and these require higher CRSS values than, say, Mg, for which the easiest one is basal slip and the CRSS value to activate it is comparatively low. The backstress can be correlated to grain neighbor orientation through its ability to activate its easiest slip or twin mode. A simple metric that quantifies alignment between the twin in the parent and a given slip mode in the neighbor is:

$$m_{rel} = \max\left((\boldsymbol{b}_T.\boldsymbol{b}_s)\,(\boldsymbol{n}_T.\boldsymbol{n}_s)\right) \tag{16}$$

where $\mathbf{b_T}$ and $\mathbf{n_T}$ are the Burgers vector and plane normal unit vector of the twin and $\mathbf{b_s}$ and $\mathbf{n_s}$ are the Burgers vector and plane normal unit vector of different slip systems of neighboring grain.

This relative neighboring grain orientation factor m_{rel} ranges from 0 to 1 and can be set as the maximum value calculated among the systems belonging to the

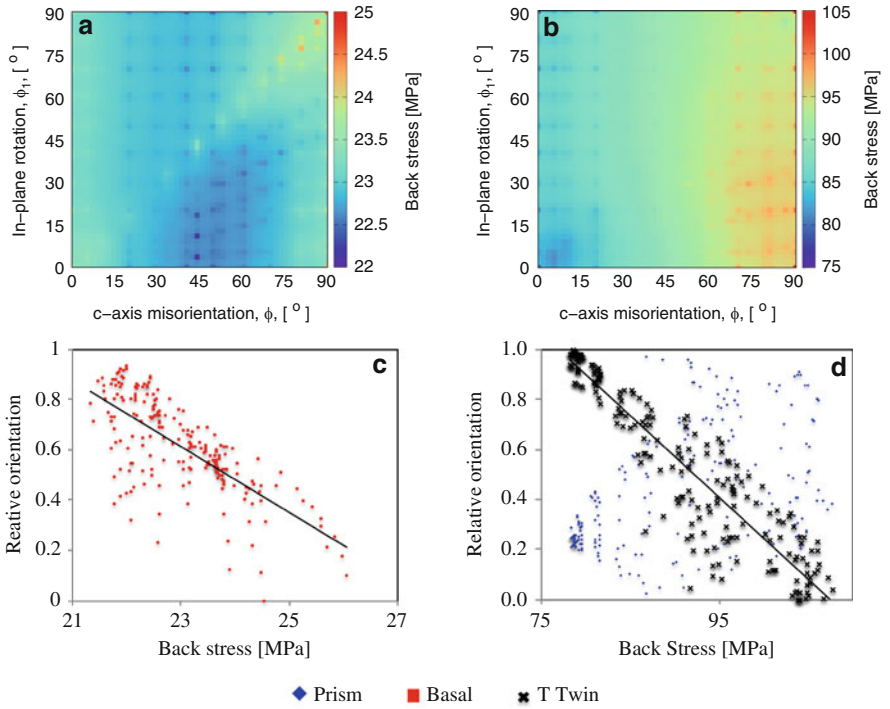

Fig. 13 Effect of neighboring grain orientation on twin backstress (Kumar et al. 2017b). Distribution of twin backstress in the neighboring grain orientation space in (**a**) Mg and (**b**) Zr. The correlation between the twin backstress and the relative orientation of primary slip system in (**c**) Mg and (**d**) Zr. In the calculations, easy basal slip systems in Mg and easy prismatic slip and tensile twin systems in Zr are shown, and the less active systems are not shown

slip family. A high $\boldsymbol{m_{rel}}$ means that the particular deformation mode is well aligned with the twin and the likely one accommodating the twin shear. Similar measures have been defined to quantify crystallographic alignment across boundaries but for different purposes, such as slip-slip transmission (Clark et al. 1992), slip-twin transmission (Wang et al. 2010b), and twin-twin transmissions (Kumar et al. 2016a, 2017a, c) across grain boundaries.

The relationships between $\boldsymbol{m_{rel}}$ for the different deformation modes and the calculated twin backstress from the CPFFT are obtained for both Mg and Zr. For pure Mg, the relationship is studied between the twin in the parent and the predominant basal slip mode in the neighbor. For Zr, the relationship is examined for both prismatic slip and the tensile twin modes. It was found that the other deformation modes are not strongly correlated with the backstress. Figure 13c shows that for Mg, the twin backstress $\boldsymbol{\tau_B}$ increases as $\boldsymbol{m_{rel}}$ for basal slip decreases. In the case of Zr, in Fig. 13d, the tensile twin mode exhibits the stronger correlation with $\boldsymbol{\tau_B}$ than prismatic slip. In particular, the correlation between $\boldsymbol{\tau_B}$ and relative

orientation of neighboring grain tensile twin $\boldsymbol{m_{TTwin}}$ is nearly linear following (see the line in Fig. 13d):

$$\tau_B = -26.63\, m_{TTwin} + 105.26 \tag{17}$$

This relationship although simple can be used in mean-field polycrystal models to indirectly account for neighborhood effects.

5.3 Incorporation of Neighborhood Effects in Homogenization Models

To simulate the role of random neighboring grain orientations on the growth of twin lamellae, the relationship expressed in Eq. (17) is incorporated into a larger scale, mean-field visco-plastic self-consistent (VPSC) model. In this hybrid VPSC model (Kumar et al. 2017b), the twin shear rate is related to the TRSS by a power-law flow rule, which introduces a resistance to twinning:

$$\dot{\gamma}^v = \dot{\gamma}_o \left(\frac{\tau^v}{\tau_c^{\text{twin}} + \tau_B} \right)^n \tag{18}$$

where $n = 20$, $\dot{\gamma}_o$ is the reference shear rate, τ^v is the TRSS of twin variant v calculated in VPSC without a neighbor effect, and τ_B is the contribution of the neighboring constraint to the resistance, the backstress we analyzed earlier with the CPFFT model.

This hybrid model is applied to polycrystalline Zr. In the simulation, for every grain, a neighboring grain orientation is randomly selected from the initial texture. Provided the grain forms a twin, its pre-assigned neighbor orientation is used to calculate the backstress on the twin using Eq. (17). Studies of the twin thickness distribution can be used to observe the effects of the neighbor on the backstress. Figure 14 compares the distribution of twin area fraction per twinned grain as a function of twin Schmid factor with the experimental measurement (see (Capolungo et al. 2009)). The model including grain neighborhood effects on twin growth reduces twinning in the high Schmid factor region yet increases it in the low Schmid factor region, providing overall better alignment with the data than the model without the effect of backstress. We find in the model that including the backstress neighbor effect lowers the growth rate *for all twins*, which is to be expected. However, in order to form the same twin fraction to accommodate the applied strain as in the model without the backstress, the lower Schmid factor twins grew to a larger volume, an interesting consequence that again, places the hybrid model calculations in better alignment with the volume fraction of these low-rank twins.

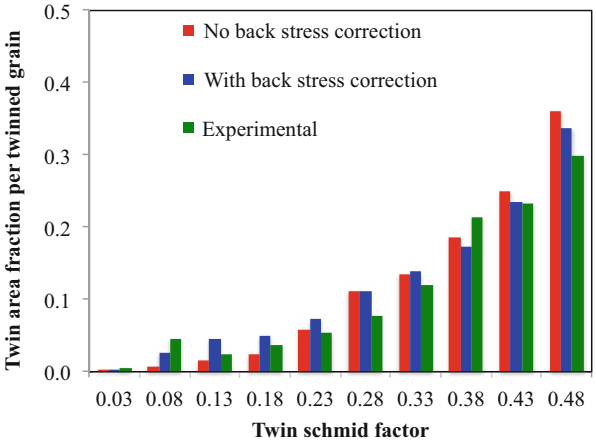

Fig. 14 Effect of the twin backstress effect when incorporated into the VPSC model (Kumar et al. 2017b). Calculated twin area distribution from the deformation of pure Zr. Including the backstress from neighboring grains reduces twinning in the high Schmid factor region and increases it in the low Schmid factor region, aligning it better with the data than the mode without the effect of the backstress

6 Conclusions and Outlook

Decades of reports from experimental analyses of deformed HCP materials have undeniably demonstrated that deformation twinning is a highly heterogeneous deformation mechanism, exhibiting significant temporal and spatial variability across the crystalline microstructures. Yet to date the fundamental understanding of the mechanistic origins of the statistical and stochastic nature of these types of twins is still in development. Considering both the growing interest in HCP materials for structural applications and the profound influence of twinning on structural response, adopting a stochastic perspective in the studies of deformation twinning during mechanical deformation is sensible. In attempt to evaluate progress toward this end, this chapter reviews recent experimental analyses and modeling efforts to describe some statistical aspects of deformation twins, correlate the more statistically variable features of twins with parent microstructure, and propose the mechanisms that explain the observed microstructure/twin relationships. The contribution of grain neighborhoods to the statistical variability, as quantified by combining experimental and modeling methods, is highlighted. In addition, recent developments of stochastic twin nucleation and growth models are presented, with the aim to determine how these stochastic aspects of twinning impact mechanical behavior. The general finding is that substantial variation in twin formation, variant selection, and size significantly impacts mechanical response, from yield and hardening to ultimate strength. These strongly suggest that future pursuits for stochastic approaches to understanding the mechanical response of HCP materials that deform via twinning are worthwhile.

There are many other very important aspects of twinning that still require study from a stochastic perspective that were not covered in this chapter. Commonly seen in HCP materials, which twin profusely, are intragranular three-dimensional networks of twins. Understanding on how these twin-twin junctions form and the variation in the types of junctions that manifest would benefit from approaches that adopt statistical descriptions and stochastic models incorporated in simulation. It should also be noted that the mechanical properties reviewed in this work pertained to responses obtained in simple loading states. Twinning microstructures are, however, sensitive to deformation temperatures and imposed strain rates and deformation histories. For instance, cyclic loading can induce phenomenon such as detwinning, or changes in strain path can cause secondary twinning. There is still much opportunity for investigating the stochastic aspects of these frequently occurring twinning events.

Acknowledgments I.J.B. acknowledges financial support from the National Science Foundation Designing Materials to Revolutionize and Engineer our Future (DMREF) program (NSF CMMI-1729887). M.A.K. acknowledges financial support from US Department of Energy, Office of Basic Energy Sciences (OBES) FWP-06SCPE401.

References

Abdolvand H, Daymond M (2013a) Multi-scale modeling and experimental study of twin inception and propagation in hexagonal close-packed materials using a crystal plasticity finite element approach-part I: average behavior. J Mech Phys Solids 61:783–802. https://doi.org/10.1016/j.jmps.2012.10.013

Abdolvand H, Daymond M (2013b) Multi-scale modeling and experimental study of twin inception and propagation in hexagonal close-packed materials using a crystal plasticity finite element approach; part II: local behavior. J Mech Phys Solids 61:803–818. https://doi.org/10.1016/j.jmps.2012.10.017

Abdolvand H, Wilkinson AJ (2016) Assessment of residual stress fields at deformation twin tips and the surrounding environments. Acta Mater 105:219–231. https://doi.org/10.1016/j.actamat.2015.11.036

Abdolvand H, Daymond M, Mareau C (2011) Incorporation of twinning into a crystal plasticity finite element model: evolution of lattice strains and texture in Zircaloy-2. Int J Plast 27:1721–1738. https://doi.org/10.1016/j.ijplas.2011.04.005

Abdolvand H et al (2015a) On the deformation twinning of Mg AZ31B: a three-dimensional synchrotron X-ray diffraction experiment and crystal plasticity finite element model. Int J Plast 70:77–97. https://doi.org/10.1016/j.ijplas.2015.03.001

Abdolvand H, Majkut M, Oddershede J, Wright J, Daymond M (2015b) Study of 3-D stress development in parent and twin pairs of a hexagonal close-packed polycrystal: part I – in-situ three-dimensional synchrotron X-ray diffraction measurement. Acta Mater 93:246–255. https://doi.org/10.1016/j.actamat.2015.04.020

Abdolvand H, Wright J, Wilkinson A (2018) Strong grain neighbour effects in polycrystals. Nat Commun 9:171. https://doi.org/10.1038/s41467-017-02213-9

Agnew SR, Brown DW, Vogel SC, Holden TM (2002) In-situ measurement of internal strain evolution during deformation dominated by mechanical twinning. In: Ecrs 6: proceedings of the 6th European conference on residual stresses, vol 404-7, pp 747–752. https://doi.org/10.4028/www.scientific.net/MSF.404-407.747

Akhtar A, Teghtsoo A (1971) Plastic deformation of Zirconium single crystals. Acta Metall Mater 19:655–663. https://doi.org/10.1016/0001-6160(71)90019-8

Ardeljan M, McCabe RJ, Beyerlein IJ, Knezevic M (2015) Explicit incorporation of deformation twins into crystal plasticity finite element models. Comput Methods Appl Mech 295:396–413. https://doi.org/10.1016/j.cma.2015.07.003

Ardeljan M, Beyerlein I, McWilliams B, Knezevic M (2016) Strain rate and temperature sensitive multi-level crystal plasticity model for large plastic deformation behavior: application to AZ31 magnesium alloy. Int J Plast 83:90–109. https://doi.org/10.1016/j.ijplas.2016.04.005

Asaro RJ (1983) Micromechanics of crystals and polycrystals. Adv Appl Mech 23:1–115. https://doi.org/10.1016/S0065-2156(08)70242-4

Asaro RJ, Lubarda VA (2006) Mechanics of solids and materials. Cambridge University Press, Cambridge/New York

Barnett MR (2007a) Twinning and the ductility of magnesium alloys part I: "Tension" twins. Mater Sci Eng A-Struct 464:1–7. https://doi.org/10.1016/j.msea.2006.12.037

Barnett MR (2007b) Twinning and the ductility of magnesium alloys part II. "Contraction" twins. Mater Sci Eng A-Struct 464:8–16. https://doi.org/10.1016/j.msea.2007.02.109

Barnett MR, Keshavarz Z, Beer AG, Atwell D (2004) Influence of grain size on the compressive deformation of wrought Mg-3Al-1Zn. Acta Mater 52:5093–5103. https://doi.org/10.1016/j.actamat.2004.07.015

Barnett MR, Nave MD, Ghaderi A (2012) Yield point elongation due to twinning in a magnesium alloy. Acta Mater 60:1433–1443. https://doi.org/10.1016/j.actamat.2011.11.022

Barrett CD, El Kadiri H (2014) The roles of grain boundary dislocations and disclinations in the nucleation of {10(1)over-bar12} twinning. Acta Mater 63:1–15. https://doi.org/10.1016/j.actamat.2013.09.012

Bay B, Hansen N, Hughes DA, Kuhlmannwilsdorf D (1992) Overview No-96 – evolution of F.C.C. deformation structures in Polyslip. Acta Metall Mater 40:205–219. https://doi.org/10.1016/0956-7151(92)90296-Q

Beyerlein IJ, Tome CN (2008) A dislocation-based constitutive law for pure Zr including temperature effects. Int J Plast 24:867–895. https://doi.org/10.1016/j.ijplas.2007.07.017

Beyerlein IJ, Tome CN (2010) A probabilistic twin nucleation model for HCP polycrystalline metals. Proc R Soc A-Math Phys 466:2517–2544. https://doi.org/10.1098/rspa.2009.0661

Beyerlein IJ, Capolungo L, Marshall PE, McCabe RJ, Tome CN (2010) Statistical analyses of deformation twinning in magnesium. Philos Mag 90:2161. https://doi.org/10.1080/14786435.2010.517966. 90:4073-4074. Pii 926495039

Beyerlein IJ, McCabe RJ, Tome CN (2011) Effect of microstructure on the nucleation of deformation twins in polycrystalline high-purity magnesium: a multi-scale modeling study. J Mech Phys Solids 59:988–1003. https://doi.org/10.1016/j.jmps.2011.02.007

Beyerlein IJ, Wang J, Barnett MR, Tome CN (2012) Double twinning mechanisms in magnesium alloys via dissociation of lattice dislocations. Proc R Soc A-Math Phys 468:1496–1520. https://doi.org/10.1098/rspa.2011.0731

Beyerlein IJ, Wang J, Kang K, Zheng SJ, Mara NA (2013) Twinnability of bimetal interfaces in nanostructured composites. Mater Res Lett 1:89–95. https://doi.org/10.1080/21663831.2013.782074

Beyerlein IJ, Zhang XH, Misra A (2014) Growth twins and deformation twins in metals. Annu Rev Mater Res 44:329–363. https://doi.org/10.1146/annurev-matsci-070813-113304

Bieler T, Wang L, Beaudoin A, Kenesei P, Lienert U (2014) In situ characterization of twin nucleation in pure Ti using 3D-XRD. Metall Mater Trans A 45A:109–122. https://doi.org/10.1007/s11661-013-2082-3

Brenner R, Lebensohn RA, Castelnau O (2009) Elastic anisotropy and yield surface estimates of polycrystals. Int J Solids Struct 46:3018–3026. https://doi.org/10.1016/j.ijsolstr.2009.04.001

Bronkhorst CA, Kalidindi SR, Anand L (1992) Polycrystalline plasticity and the evolution of crystallographic texture in Fcc metals. Philos Trans R Soc A 341:443–477. https://doi.org/10.1098/rsta.1992.0111

Canova GR, Fressengeas C, Molinari A, Kocks UF (1988) Effect of rate sensitivity on slip system activity and lattice rotation. Acta Metall Mater 36:1961–1970. https://doi.org/10.1016/0001-6160(88)90298-2

Capolungo L, Beyerlein IJ (2008) Nucleation and stability of twins in hcp metals. Phys Rev B 78:024117. https://doi.org/10.1103/PhysRevB.78.024117. ARTN 024117

Capolungo L, Marshall PE, McCabe RJ, Beyerlein IJ, Tome CN (2009) Nucleation and growth of twins in Zr: a statistical study. Acta Mater 57:6047–6056. https://doi.org/10.1016/j.actamat.2009.08.030

Cheng JH, Ghosh S (2015) A crystal plasticity FE model for deformation with twin nucleation in magnesium alloys. Int J Plast 67:148–170. https://doi.org/10.1016/j.ijplas.2014.10.005

Cheng JH, Ghosh S (2017a) Crystal plasticity finite element modeling of discrete twin evolution in polycrystalline magnesium. J Mech Phys Solids 99:512–538. https://doi.org/10.1016/j.jmps.2016.12.008

Cheng JH, Ghosh S (2017b) Simulating discrete twin evolution in magnesium using a novel crystal plasticity finite element model. Miner Met Mater Ser:167–174. https://doi.org/10.1007/978-3-319-52392-7_26

Clark WAT, Wagoner RH, Shen ZY, Lee TC, Robertson IM, Birnbaum HK (1992) On the criteria for slip transmission across interfaces in polycrystals. Scr Metall Mater 26:203–206. https://doi.org/10.1016/0956-716x(92)90173-C

Cohen JB, Weertman J (1963) A dislocation model for twinning in F.C.C. Metals. Acta Metall Mater 11:996. https://doi.org/10.1016/0001-6160(63)90074-9

Delannay L, Jacques PJ, Kalidindi SR (2006) Finite element modeling of crystal plasticity with grains shaped as truncated octahedrons. Int J Plast 22:1879–1898. https://doi.org/10.1016/j.ijplas.2006.01.008

Ecob N, Ralph B (1983) The effect of grain-size on deformation twinning in a textured zinc alloy. J Mater Sci 18:2419–2429. https://doi.org/10.1007/Bf00541848

Eisenlohr P, Diehl M, Lebensohn RA, Roters F (2013) A spectral method solution to crystal elasto-viscoplasticity at finite strains. Int J Plast 46:37–53. https://doi.org/10.1016/j.ijplas.2012.09.012

Fisher ES, Renken CJ (1964) Single-Crystal Elastic Moduli + Hcp to Bcc Transformation in Ti,Zr, + Hf. Phys Rev A-Gen Phys 135:A482–A494. https://doi.org/10.1103/PhysRev.135.A482

Ghaderi A, Barnett M (2011) Sensitivity of deformation twinning to grain size in titanium and magnesium. Acta Mater 59:7824–7839. https://doi.org/10.1016/j.actamat.2011.09.018

Gutierrez-Urrutia I, Raabe D (2012) Grain size effect on strain hardening in twinning-induced plasticity steels. Scr Mater 66:992–996. https://doi.org/10.1016/j.scriptamat.2012.01.037

Hazeli K, Cuadra J, Vanniamparambil PA, Kontsos A (2013) In situ identification of twin-related bands near yielding in a magnesium alloy. Scr Mater 68:83–86. https://doi.org/10.1016/j.scriptamat.2012.09.009

Hearmon RFS (1946) The elastic constants of anisotropic materials. Rev Mod Phys 18:409–440. https://doi.org/10.1103/RevModPhys.18.409

Hosford WF (1993) The mechanics of crystals and textured polycrystals. The Oxford engineering science series, vol 32. Oxford University Press, New York

Hughes DA, Hansen N (1997) High angle boundaries formed by grain subdivision mechanisms. Acta Mater 45:3871–3886. https://doi.org/10.1016/S1359-6454(97)00027-X

Idiart MI, Moulinec H, Castaneda PP, Suquet P (2006) Macroscopic behavior and field fluctuations in viscoplastic composites: second-order estimates versus full-field simulations. J Mech Phys Solids 54:1029–1063. https://doi.org/10.1016/j.jmps.2005.11.004

Jagannadham K (1976) Lattice dislocation near a surface. J Appl Phys 47:4401–4403. https://doi.org/10.1063/1.322445

Jain A, Duygulu O, Brown DW, Tome CN, Agnew SR (2008) Grain size effects on the tensile properties and deformation mechanisms of a magnesium alloy, AZ31B, sheet. Mat Sci Eng A-Struct 486:545–555. https://doi.org/10.1016/j.msea.2007.09.069

Juan PA, Pradalier C, Berbenni S, McCabe RJ, Tome CN, Capolungo L (2015) A statistical analysis of the influence of microstructure and twin-twin junctions on twin nucleation and twin growth in Zr. Acta Mater 95:399–410. https://doi.org/10.1016/j.actamat.2015.05.022

Kacher J, Minor AM (2014) Twin boundary interactions with grain boundaries investigated in pure rhenium. Acta Mater 81:1–8. https://doi.org/10.1016/j.actamat.2014.08.013

Kalidindi SR (1998) Incorporation of deformation twinning in crystal plasticity models. J Mech Phys Solids 46:267–290. https://doi.org/10.1016/S0022-5096(97)00051-3

Kang S, Jung JG, Kang M, Woo W, Lee YK (2016) The effects of grain size on yielding, strain hardening, and mechanical twinning in Fe-18Mn-0.6C-1.5Al twinning-induced plasticity steel. Mat Sci Eng A-Struct 652:212–220. https://doi.org/10.1016/j.msea.2015.11.096

Kanjarla AK, Beyerlein IJ, Lebensohn RA, Tome CN (2012a) On the role of local grain interactions on twin nucleation and texture evolution in hexagonal materials. Mater Sci Forum 702-703:265–268. https://doi.org/10.4028/www.scientific.net/MSF.702-703.265

Kanjarla AK, Lebensohn RA, Balogh L, Tome CN (2012b) Study of internal lattice strain distributions in stainless steel using a full-field elasto-viscoplastic formulation based on fast Fourier transforms. Acta Mater 60:3094–3106. https://doi.org/10.1016/j.actamat.2012.02.014

Kaschner GC, Tome CN, Beyerlein IJ, Vogel SC, Brown DW, McCabe RJ (2006) Role of twinning in the hardening response of zirconium during temperature reloads. Acta Mater 54:2887–2896. https://doi.org/10.1016/j.actamat.2006.02.036

Khosravani A, Fullwood DT, Adams BL, Rampton TM, Miles MP, Mishra RK (2015) Nucleation and propagation of {1 0(1)over-bar2} twins in AZ31 magnesium alloy. Acta Mater 100:202–214. https://doi.org/10.1016/j.actamat.2015.08.024

Knezevic M, Zecevic M, Beyerlein I, Bingert J, McCabe R (2015) Strain rate and temperature effects on the selection of primary and secondary slip and twinning systems in HCP Zr. Acta Mater 88:55–73. https://doi.org/10.1016/j.actamat.2015.01.037

Knezevic M, Zecevic M, Beyerlein I, Lebensohn R (2016) A numerical procedure enabling accurate descriptions of strain rate-sensitive flow of polycrystals within crystal visco-plasticity theory. Comput Method Appl Mech 308:468–482. https://doi.org/10.1016/j.cma.2016.05.025

Kocks UF (1970) Relation between Polycrystal deformation and single-crystal deformation. Metall Trans 1:1121–1143. https://doi.org/10.1007/Bf02900224

Kocks UF, Tomé CN, Wenk HR (2000) Texture and anisotropy – preferred orientations in polycrystals and their effect on materials properties. Cambridge University Press, Cambridge

Kuhlmann-Wilsdorf D (1999) Overview no. 131 – "Regular" deformation bands (DBs) and the LEDS hypothesis. Acta Mater 47:1697–1712. https://doi.org/10.1016/S1359-6454(98)00413-3

Kuhlman-wilsdorf D, Hansen N (1991) Geometrically necessary, incidental and subgrain boundaries. Scr Metall Mater 25:1557–1562. https://doi.org/10.1016/0956-716x(91)90451-6

Kumar MA, Mahesh S (2012) Banding in single crystals during plastic deformation. Int J Plast 36:15–33. https://doi.org/10.1016/j.ijplas.2012.03.008

Kumar MA, Kanjarla AK, Niezgoda SR, Lebensohn RA, Tome CN (2015) Numerical study of the stress state of a deformation twin in magnesium. Acta Mater 84:349–358. https://doi.org/10.1016/j.actamat.2014.10.048

Kumar MA, Beyerlein IJ, McCabe RJ, Tome CN (2016a) Grain neighbour effects on twin transmission in hexagonal close-packed materials. Nat Commun 7. https://doi.org/10.1038/ncomms13826. ARTN 13826

Kumar MA, Beyerlein IJ, Tome CN (2016b) Effect of local stress fields on twin characteristics in HCP metals. Acta Mater 116:143–154. https://doi.org/10.1016/j.actamat.2016.06.042

Kumar MA, Beyerlein IJ, Tome CN (2016c) Grain size constraints on twin expansion in hexagonal close packed crystals. J Appl Phys 120. https://doi.org/10.1063/1.4965719. Artn 155105

Kumar MA, Beyerlein IJ, Lebensohn RA, Tome CN (2017a) Modeling the effect of alloying elements in magnesium on deformation twin characteristics. Miner Met Mater Ser:159–165. https://doi.org/10.1007/978-3-319-52392-7_25

Kumar MA, Beyerlein IJ, Lebensohn RA, Tome CN (2017b) Modeling the effect of neighboring grains on twin growth in HCP polycrystals. Model Simul Mater Sci 25. https://doi.org/10.1088/1361-651X/aa7bbb. ARTN 064007

Kumar MA, Beyerlein IJ, Lebensohn RA, Tome CN (2017c) Role of alloying elements on twin growth and twin transmission in magnesium alloys. Mat Sci Eng A-Struct 706:295–303. https://doi.org/10.1016/j.msea.2017.08.084

Kumar MA, Beyerlein IJ, Tome CN (2017d) A measure of plastic anisotropy for hexagonal close packed metals: application to alloying effects on the formability of Mg. J Alloys Compd 695:1488–1497. https://doi.org/10.1016/j.jallcom.2016.10.287

Kumar MA, Wroński M, McCabe RJ, Capolungo L, Wierzbanowski K, Tomé CN (2018) Role of microstructure on twin nucleation and growth in HCP titanium: a statistical study. Acta Mater 148:123–132

Lebensohn RA (2001) N-site modeling of a 3D viscoplastic polycrystal using fast Fourier transform. Acta Mater 49:2723–2737

Lebensohn RA, Tome CN (1993) A self-consistent anisotropic approach for the simulation of plastic-deformation and texture development of polycrystals – application to zirconium alloys. Acta Metall Mater 41:2611–2624. https://doi.org/10.1016/0956-7151(93)90130-K

Lebensohn RA, Brenner R, Castelnau O, Rollett AD (2008) Orientation image-based micromechanical modelling of subgrain texture evolution in polycrystalline copper. Acta Mater 56:3914–3926. https://doi.org/10.1016/j.actamat.2008.04.016

Lebensohn RA, Castañeda PP, Brenner R, Castelnau O (2011a) Full-field vs. homogenization methods to predict microstructure–property relations for polycrystalline materials. In: Ghosh S, Dimiduk D (eds) Computational methods for microstructure-property relationships. Springer, Boston

Lebensohn RA, Idiart MI, Castaneda PP, Vincent PG (2011b) Dilatational viscoplasticity of polycrystalline solids with intergranular cavities. Philos Mag 91:3038–3067. https://doi.org/10.1080/14786435.2011.561811

Lebensohn RA, Kanjarla AK, Eisenlohr P (2012) An elasto-viscoplastic formulation based on fast Fourier transforms for the prediction of micromechanical fields in polycrystalline materials. Int J Plast 32–33:59–69. https://doi.org/10.1016/j.ijplas.2011.12.005

Lentz M, Behringer A, Fahrenson C, Beyerlein IJ, Reimers W (2014) Grain size effects on primary, secondary, and tertiary twin development in Mg-4 wt pct Li (-1 wt pct Al) alloys. Metall Mater Trans A 45a:4737–4741. https://doi.org/10.1007/s11661-014-2491-y

Lentz M, Klaus M, Beyerlein IJ, Zecevic M, Reimers W, Knezevic M (2015) In situ X-ray diffraction and crystal plasticity modeling of the deformation behavior of extruded Mg-Li-(Al) alloys: an uncommon tension-compression asymmetry. Acta Mater 86:254–268. https://doi.org/10.1016/j.actamat.2014.12.003

Lentz M, Risse M, Schaefer N, Reimers W, Beyerlein IJ (2016) Strength and ductility with {10(1)over-bar1} – {10(1)over-bar2} double twinning in a magnesium alloy. Nat Commun 7. https://doi.org/10.1038/ncomms11068. ARTN 11068

Liu B, Raabe D, Roters F, Eisenlohr P, Lebensohn RA (2010) Comparison of finite element and fast Fourier transform crystal plasticity solvers for texture prediction. Model Simul Mater Sci 18. https://doi.org/10.1088/0965-0393/18/8/085005. Artn 085005

Liu X, Nuhfer NT, Warren AP, Coffey KR, Rohrer GS, Barmak K (2015) Grain size dependence of the twin length fraction in nanocrystalline Cu thin films via transmission electron microscopy based orientation mapping. J Mater Res 30:528–537. https://doi.org/10.1557/jmr.2014.393

Mahajan S, Chin GY (1973) Formation of deformation twins in Fcc crystals. Acta Metall Mater 21:1353–1363. https://doi.org/10.1016/0001-6160(73)90085-0

Masson R, Bornert M, Suquet P, Zaoui A (2000) An affine formulation for the prediction of the effective properties of nonlinear composites and polycrystals. J Mech Phys Solids 48:1203–1227. https://doi.org/10.1016/S0022-5096(99)00071-X

McCabe RJ, Proust G, Cerreta EK, Misra A (2009) Quantitative analysis of deformation twinning in zirconium. Int J Plast 25:454–472. https://doi.org/10.1016/j.ijplas.2008.03.010

Mendelson S (1972) Dislocation dissociations and dislocation mobility in diamond lattice crystals. J Appl Phys 43:2102. https://doi.org/10.1063/1.1661460

Michel J, Moulinec H, Suquet P (2000) A computational method based on augmented Lagrangians and fast Fourier transforms for composites with high contrast. Comput Model Eng Sci 1:79–88

Michel J, Moulinec H, Suquet P (2001) A computational scheme for linear and non-linear composites with arbitrary phase contrast. Int J Numer Methods Eng 52:139–158. https://doi.org/10.1002/nme.275

Mika D, Dawson P (1999) Polycrystal plasticity modeling of intracrystalline boundary textures. Acta Mater 47:1355–1369. https://doi.org/10.1016/S1359-6454(98)00386-3

Morrow BM, Cerreta EK, McCabe RJ, Tome CN (2014a) Toward understanding twin-twin interactions in hcp metals: utilizing multiscale techniques to characterize deformation mechanisms in magnesium. Mater Sci Eng A-Struct 613:365–371. https://doi.org/10.1016/j.msea.2014.06.062

Morrow BM, Mccabe RJ, Cerreta EK, Tome CN (2014b) In-situ TEM observation of twinning and detwinning during cyclic loading in Mg. Metall Mater Trans A 45a:36–40. https://doi.org/10.1007/s11661-013-1765-0

Morrow BM, McCabe RJ, Cerreta EK, Tome CN (2014c) Observations of the atomic structure of tensile and compressive twin boundaries and twin-twin interactions in zirconium. Metall Mater Trans A 45a:5891–5897. https://doi.org/10.1007/s11661-014-2481-0

Moulinec H, Suquet P (1994) A fast numerical method for computing the linear and nonlinear mechanical properties of composites. C R Acad Sci Ser II 318:1417–1423

Moulinec H, Suquet P (1998) A numerical method for computing the overall response of nonlinear composites with complex microstructure. Comput Method Appl Mech 157:69–94. https://doi.org/10.1016/S0045-7825(97)00218-1

Niezgoda SR, Beyerlein IJ, Kanjarla AK, Tome CN (2013) Introducing grain boundary influenced stochastic effects into constitutive models. Jom-Us 65:419–430. https://doi.org/10.1007/s11837-012-0550-7

Niezgoda SR, Kanjarla AK, Beyerlein IJ, Tome CN (2014) Stochastic modeling of twin nucleation in polycrystals: an application in hexagonal close-packed metals. Int J Plast 56:119–138. https://doi.org/10.1016/j.ijplas.2013.11.005

Partridge PG (1967) The crystallography and deformation modes of hexagonal close-packed metals. Metall Rev 12:169–194

Peirce D, Asaro RJ, Needleman A (1982) An analysis of nonuniform and localized deformation in ductile single-crystals. Acta Metall Mater 30:1087–1119. https://doi.org/10.1016/0001-6160(82)90005-0

Priestner R, Leslie WC (1965) Nucleation of deformation twins at slip plane intersections in Bcc metals. Philos Mag 11:895–916. https://doi.org/10.1080/14786436508223953

Proust G, Tome CN, Kaschner GC (2007) Modeling texture, twinning and hardening evolution during deformation of hexagonal materials. Acta Mater 55:2137–2148. https://doi.org/10.1016/j.actamat.2006.11.017

Proust G, Tome CN, Jain A, Agnew SR (2009) Modeling the effect of twinning and detwinning during strain-path changes of magnesium alloy AZ31. Int J Plast 25:861–880. https://doi.org/10.1016/j.ijplas.2008.05.005

Rahman KM, Vorontsov VA, Dye D (2015) The effect of grain size on the twin initiation stress in a TWIP steel. Acta Mater 89:247–257. https://doi.org/10.1016/j.actamat.2015.02.008

Roters F, Eisenlohr P, Hantcherli L, Tjahjanto DD, Bieler TR, Raabe D (2010) Overview of constitutive laws, kinematics, homogenization and multiscale methods in crystal plasticity finite-element modeling: theory, experiments, applications. Acta Mater 58:1152–1211. https://doi.org/10.1016/j.actamat.2009.10.058

Salem AA, Kalidindi SR, Doherty RD, Semiatin SL (2006) Strain hardening due to deformation twinning in alpha-titanium: Mechanisms. Metall Mater Trans A 37a:259–268. https://doi.org/10.1007/s11661-006-0171-2

Shanthraj P, Eisenlohr P, Diehl M, Roters F (2015) Numerically robust spectral methods for crystal plasticity simulations of heterogeneous materials. Int J Plast 66:31–45. https://doi.org/10.1016/j.ijplas.2014.02.006

Shi ZZ et al (2015a) On the selection of extension twin variants with low Schmid factors in a deformed Mg alloy. Acta Mater 83:17–28. https://doi.org/10.1016/j.actamat.2014.10.004

Shi ZZ et al (2015b) Variant selection of twins with low Schmid factors in cross grain boundary twin pairs in a magnesium alloy. Iop Conf Ser-Mat Sci 82. https://doi.org/10.1088/1757-899x/82/1/012021. Artn 012021

Shi ZZ et al (2015c) Sequential double extension twinning in a magnesium alloy: combined statistical and micromechanical analyses. Acta Mater 96:333–343. https://doi.org/10.1016/j.actamat.2015.06.029

Simkin BA, Ng BC, Crimp MA, Bieler TR (2007) Crack opening due to deformation twin shear at grain boundaries in near-gamma TiAl. Intermetallics 15:55–60. https://doi.org/10.1016/j.intermet.2006.03.005

Simmons G, Wang H (1971) Single crystal elastic constants and calculated aggregate properties: a handbook. MIT press, Cambridge, MA

Stanford N, Barnett MR (2008) Fine grained AZ31 produced by conventional thermo-mechanical processing. J Alloys Compd 466:182–188. https://doi.org/10.1016/j.jallcom.2007.11.082

Thorvaldsen A (1993) Grain-growth as a stochastic process. Acta Metall Mater 41:1347–1357. https://doi.org/10.1016/0956-7151(93)90244-M

Tome C, Canova GR, Kocks UF, Christodoulou N, Jonas JJ (1984) The relation between macroscopic and microscopic strain-hardening in Fcc polycrystals. Acta Metall Mater 32:1637–1653. https://doi.org/10.1016/0001-6160(84)90222-0

Tome C, Lebensohn R, Kocks U (1991) A model for texture development dominated by deformation twinning – application to zirconium alloys. Acta Metall Mater 39:2667–2680. https://doi.org/10.1016/0956-7151(91)90083-D

Tsai MS, Chang CP (2013) Grain size effect on deformation twinning in Mg-Al-Zn alloy. Mater Sci Technol-Lond 29:759–763. https://doi.org/10.1179/1743284713y.0000000237

Wang J, Beyerlein IJ, Tome CN (2010a) An atomic and probabilistic perspective on twin nucleation in Mg. Scr Mater 63:741–746. https://doi.org/10.1016/j.scriptamat.2010.01.047

Wang L, Yang Y, Eisenlohr P, Bieler TR, Crimp MA, Mason DE (2010b) Twin nucleation by slip transfer across grain boundaries in commercial purity titanium. Metall Mater Trans A 41a:421–430. https://doi.org/10.1007/s11661-009-0097-6

Wang J, Beyerlein IJ, Hirth JP, Tome CN (2011) Twinning dislocations on {(1)over-bar011} and {(1)over-bar013} planes in hexagonal close-packed crystals. Acta Mater 59:3990–4001. https://doi.org/10.1016/j.actamat.2011.03.024

Wang J, Beyerlein IJ, Hirth JP (2012) Nucleation of elementary {(1)over-bar 0 1 1} and {(1)over-bar 0 1 3} twinning dislocations at a twin boundary in hexagonal close-packed crystals. Model Simul Mater Sci 20:024001. https://doi.org/10.1088/0965-0393/20/2/024001

Wang H, Wu PD, Wang J, Tome CN (2013a) A crystal plasticity model for hexagonal close packed (HCP) crystals including twinning and de-twinning mechanisms. Int J Plast 49:36–52. https://doi.org/10.1016/j.ijplas.2013.02.016

Wang J, Yadav SK, Hirth JP, Tome CN, Beyerlein IJ (2013b) Pure-shuffle nucleation of deformation twins in hexagonal-close-packed metals. Mater Res Lett 1:126–132. https://doi.org/10.1080/21663831.2013.792019

Wang LY, Barabash R, Bieler T, Liu WJ, Eisenlohr P (2013c) Study of twinning in alpha-Ti by EBSD and Laue microdiffraction. Metall Mater Trans A 44a:3664–3674. https://doi.org/10.1007/s11661-013-1714-y

Wang J, Beyerlein IJ, Tome CN (2014) Reactions of lattice dislocations with grain boundaries in Mg: implications on the micro scale from atomic-scale calculations. Int J Plast 56:156–172. https://doi.org/10.1016/j.ijplas.2013.11.009

Wongwiwat K, Murr LE (1978) Effect of shock pressure, pulse duration, and grain-size on shock-deformation twinning in molybdenum. Mater Sci Eng 35:273–285. https://doi.org/10.1016/0025-5416(78)90129-5

Wronski M, Arul Kumar M, Capolungo L, Madec R, Wierzbanowski K, Tome CN (2018) Deformation behavior of CP-titanium: experiment and crystal plasticity modeling. Mater Sci Eng A-Struct 724:289–297

Wu W, Chuang CP, Qiao DX, Ren Y, An K (2016) Investigation of deformation twinning under complex stress states in a rolled magnesium alloy. J Alloys Compd 683:619–633. https://doi.org/10.1016/j.jallcom.2016.05.144

Yang F, Yin SM, Li SX, Zhang ZF (2008) Crack initiation mechanism of extruded AZ31 magnesium alloy in the very high cycle fatigue regime. Mater Sci Eng A-Struct 491:131–136. https://doi.org/10.1016/j.msea.2008.02.003

Yin SM, Yang F, Yang XM, Wu SD, Li SX, Li GY (2008) The role of twinning-detwinning on fatigue fracture morphology of Mg-3%Al-1%Zn alloy. Mater Sci Eng A-Struct 494:397–400. https://doi.org/10.1016/j.msea.2008.04.056

Yoo MH (1981) Slip, twinning, and fracture in hexagonal close-packed metals. Metall Trans A 12:409–418. https://doi.org/10.1007/Bf02648537

Yoo MH, Lee JK (1991) Deformation twinning in Hcp metals and alloys. Philos Mag A 63:987–1000. https://doi.org/10.1080/01418619108213931

Zecevic M, Knezevic M (2017) Modeling of sheet metal forming based on implicit embedding of the elasto-plastic self-consistent formulation in shell elements: application to cup drawing of AA6022-T4. Jom-Us 69:922–929. https://doi.org/10.1007/s11837-017-2255-4

Zhao Z, Kuchnicki S, Radovitzky R, Cultino A (2007) Influence of in-grain mesh resolution on the prediction of deformation textures in fcc polycrystals by crystal plasticity FEM. Acta Mater 55:2361–2373. https://doi.org/10.1016/j.actamat.2006.11.035

Zheng SJ, Beyerlein IJ, Wang J, Carpenter JS, Han WZ, Mara NA (2012) Deformation twinning mechanisms from bimetal interfaces as revealed by in situ straining in the TEM. Acta Mater 60:5858–5866. https://doi.org/10.1016/j.actamat.2012.07.027